

5-Phenyl-1,3,4-oxadiazol-2(3H)-ones are potent inhibitors of Notum carboxylesterase activity identified by the optimization of a crystallographic fragment screening hit.

William Mahy,^{1,†} Nicky J. Willis,^{1,†} Yuguang Zhao,^{2,†} Hannah L. Woodward,¹ Fredrik Svensson,^{1,3} James Siphthorp,^{1,3} Luca Vecchia,² Reinis R. Ruza,² James Hillier,² Svend Kjaer,³ Sarah Frew,¹ Amy Monaghan,¹ Magda Bictash,¹ Patricia Salinas,⁴ Paul Whiting,¹ Jean-Paul Vincent,³ E. Yvonne Jones,^{2,*} Paul V. Fish.^{1,3,*}

¹ Alzheimer's Research UK UCL Drug Discovery Institute, University College London, Cruciform Building, Gower Street, London, WC1E 6BT, U.K.

² Division of Structural Biology, Wellcome Centre for Human Genetics, University of Oxford, The Henry Wellcome Building for Genomic Medicine, Roosevelt Drive, Oxford, OX3 7BN, U.K.

³ The Francis Crick Institute, 1 Midland Road, Kings Cross, London NW1 1AT, U.K.

⁴ Department of Cell and Developmental Biology, Laboratory for Molecular and Cellular Biology, University College London, London, WC1E 6BT, U.K.

Abstract

Carboxylesterase Notum is a negative regulator of the Wnt signaling pathway. There is an emerging understanding of the role Notum plays in disease supporting the need to discover new small molecule inhibitors. A crystallographic x-ray fragment screen was performed, which identified fragment hit 1,2,3-triazole **7** as an attractive starting point for a structure-based drug design hit-to-lead program. Optimization of **7** identified oxadiazol-2-one **23dd** as a preferred example with properties consistent with drug-like chemical space. Screening **23dd** in a cell-based TCF/LEF reporter gene assay restored activation of Wnt signaling in the presence of Notum. Mouse pharmacokinetic studies with oral administration of **23dd** demonstrated good plasma exposure and partial blood-brain barrier penetration. Significant progress was made in developing fragment hit **7** into lead **23dd** (>600-fold increase in activity) making it suitable as a new chemical tool for exploring the role of Notum mediated regulation of Wnt signaling.

Keywords: Notum inhibitor, Wnt signaling, x-ray fragment screen, structure-based drug design, 5-phenyl-1,3,4-oxadiazol-2(3H)-one, blood-brain barrier.

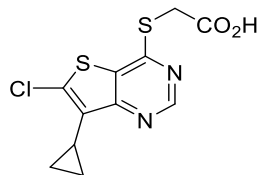
INTRODUCTION

The Wnt signaling system plays an essential role in both development and adult mammalian biology.¹ Its dysregulation in a number of diseases, including cancer² and osteoporosis,³ has led to significant interest in constituents of the Wnt pathway as drug targets. Indeed, a number of Wnt-targeted cancer therapies are in clinical development.⁴ However, targeting the Wnt signaling system has proven to be challenging as some of the targets would not be defined as “classically druggable”. Notum, a secreted palmitoleoyl-protein carboxylesterase, has recently been identified as a negative modulator of Wnt signaling.⁵ Notum acts through the removal of an essential palmitoyl moiety from Wnt proteins, thereby rendering them inactive. As an enzyme with a defined high resolution crystal structure,⁵ it may present a more tractable drug target for modulating Wnt signaling.

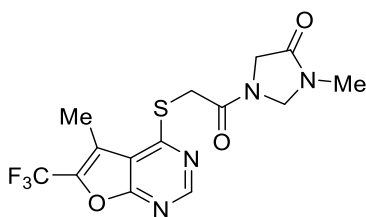
Greater understanding of the biological role of Notum makes targeting this enzyme a potential therapeutic approach for treating an increasing number of diseases. For example, using both genetic and pharmacological approaches, the inactivation of Notum secreted by osteoblasts led to an increase in cortical bone mass, suggesting a therapeutic opportunity in osteoporosis.^{6,7} In the intestinal crypt, the expression of Notum by Paneth cells increases with age, leading to decreased Wnt signaling and subsequent reduction in stem cell maintenance. A small molecule Notum inhibitor normalized Wnt signaling and restored epithelial regeneration, suggesting a therapeutic opportunity for restoration of aged or damaged tissue.⁸ In the brain, Wnt signaling is known to be a key modulator of synapse number and function,⁹ which is thought to be impaired in Alzheimer’s disease (AD),¹⁰ although a role for Notum in this process has yet to be described. Notum has however been demonstrated to play an important role in regulating neurogenesis in the brain, presumably by modulating Wnt signaling.¹¹ Thus while speculative, inhibiting Notum would be expected to increase neurogenesis, and may have potential as a regenerative therapy in acute and chronic neurological and neurodegenerative disease.¹²

There are now inhibitors of Notum carboxylesterase activity providing chemical tools for use in target validation experiments (**1-6**; **Figure 1**).¹³⁻¹⁹ A few of these inhibitors have been evaluated in mouse pharmacodynamics (PD) and pharmacokinetic (PK) studies, and show good plasma levels but limited brain exposure. Thieno[3,2-*d*]pyrimidine **LP-922056 (1)** has shown utility in mouse models of bone growth and found to increase cortical bone thickness.^{7,13} Although **1** demonstrates good oral bioavailability, additional pharmacokinetic studies in mouse showed negligible brain exposure.²⁰ Scaffold-hopping from acid **1** identified amide **2** as a potent inhibitor of Notum.¹⁴ Pharmacokinetic studies in mouse with oral administration of **2** showed improved brain penetration with a brain:plasma concentration ratio of 0.29.¹⁴ *N*-Hydroxyhydantoin carbamate **ABC99 (3)** is a potent and selective irreversible inhibitor of Notum discovered by activity-based protein profiling (ABPP).¹⁵ Inhibition of Notum in mice with **3** enhanced the regenerative capacity of aged intestinal stem cells and promoted recovery from chemotherapy-induced damage.⁸ In their study, mice were injected intraperitoneally with **3** daily for 8 days, although no drug levels were reported.⁸ These chemical tools are potentially suitable for use to explore the impact of Notum inhibition in models of peripheral disease but unlikely to be of use in models of central nervous system (CNS) disease where blood-brain barrier (BBB) permeability is an essential requirement.

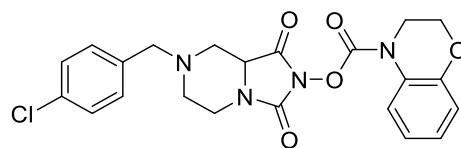
Hence, our objective was to discover new small molecule inhibitors of Notum activity suitable for exploring the regulation of Wnt signaling in the CNS and, ultimately, demonstration of modulation of AD phenotypes in cellular and mouse models. We adopted a strategy to explore complementary hit-finding approaches to identify multiple chemotypes in order to increase our chances of delivering a 'fit-for-purpose' chemical tool. Prior art has shown the success of high-throughput screening (HTS) campaigns¹³ and ABPP¹⁵ to identify inhibitors of Notum. Our own work has demonstrated that quality hits can be identified by fragment screening.¹⁶⁻¹⁸



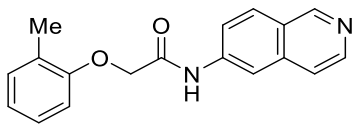
1: LP-922056
 $IC_{50} 1.1 \pm 0.4 \text{ nM}^a$



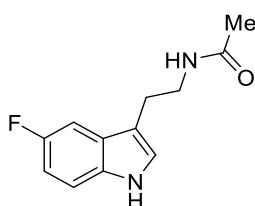
2
 $IC_{50} 3.9 \pm 0.8 \text{ nM}^a$



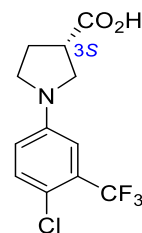
3: ABC99
 $IC_{50} 13 \text{ nM}^b$
 $IC_{50} 170 \pm 20 \text{ nM}^{a,c}$



4
 $IC_{50} 85 \pm 11 \text{ nM}^a$



5
 $IC_{50} 37,200 \text{ nM}^d$



6
 $IC_{50} 110 \pm 10 \text{ nM}^a$

Figure 1: Chemical structures and IC_{50} values of Notum inhibitors

^a Notum IC_{50} data presented in Figure 1 and Tables 1-4 are for comparison in a common assay format. This work unless otherwise stated.

^b Determined by competitive gel-based activity-based protein profiling (ABPP), see reference 15.

^c As a covalent inhibitor of Notum, the IC_{50} value will be time dependent.

^d See reference 17.

RESULTS and DISCUSSION

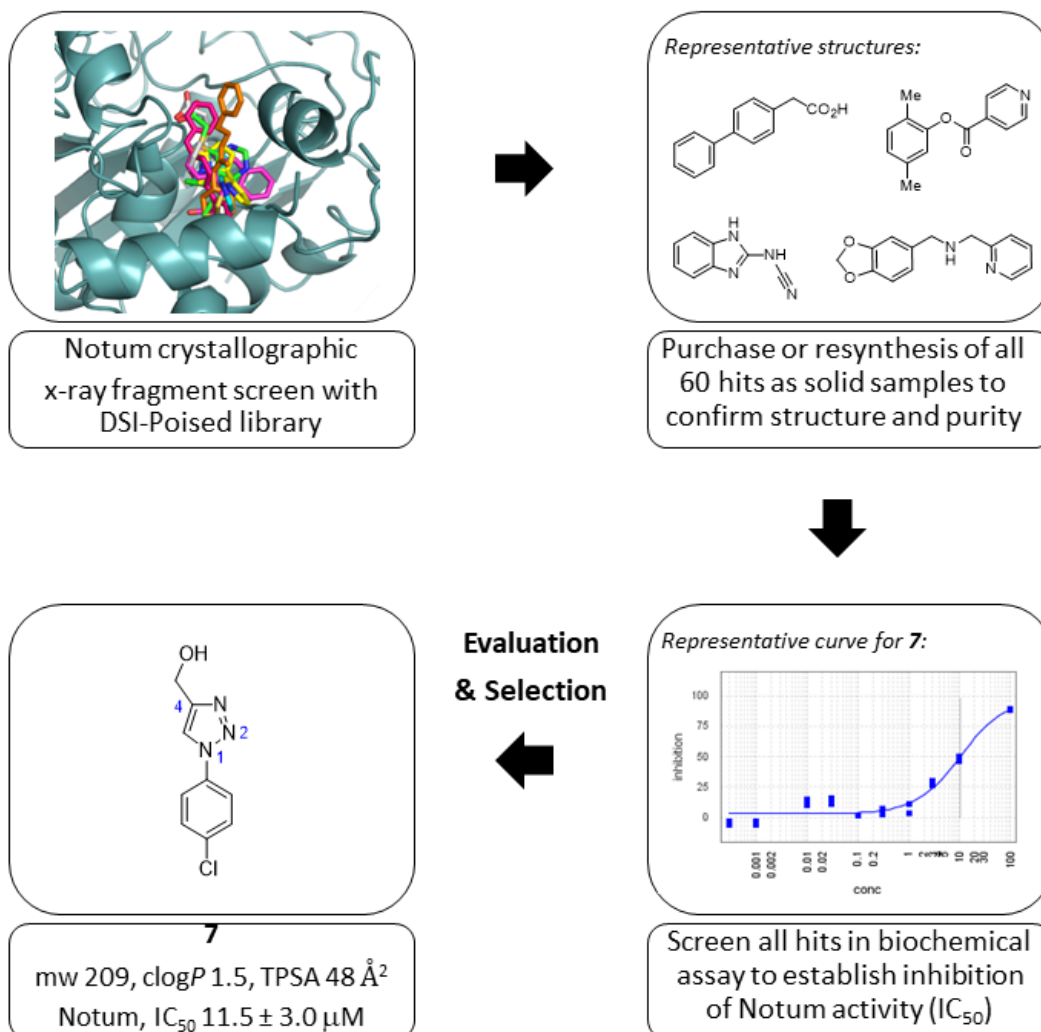
In order to identify new small molecule inhibitors of Notum, a crystallographic fragment screen was performed using the XChem platform at Diamond Light Source (Oxford, UK).^{16,17} Crystals of C-terminal His-tagged Notum(Ser81-Thr451 Cys330Ser) were soaked with the original DSI-Poised library (XChem, 768 fragments, acoustically dispensed as singletons).^{17,21} Notum has a well-defined, large, hydrophobic active-site pocket adjacent to the catalytic triad (Ser232, His389, Asp340) that accommodates the palmitoleate group of Wnt.⁵ Sixty fragments were found to bind in this pocket (hit rate: 7.8 %) with a diverse mixture of chemical structures and classes (acids, bases and neutrals) including small clusters of structurally related hits (**Figure 2**). These fragment hits were all resupplied as solid samples by purchase or re-synthesis to establish structure and purity.

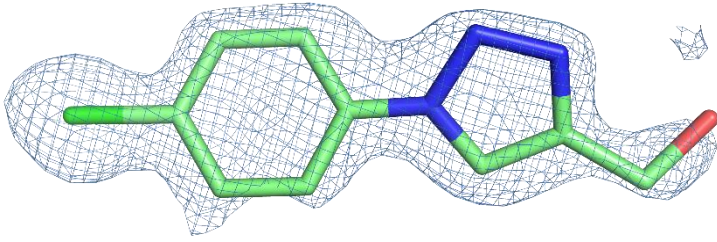
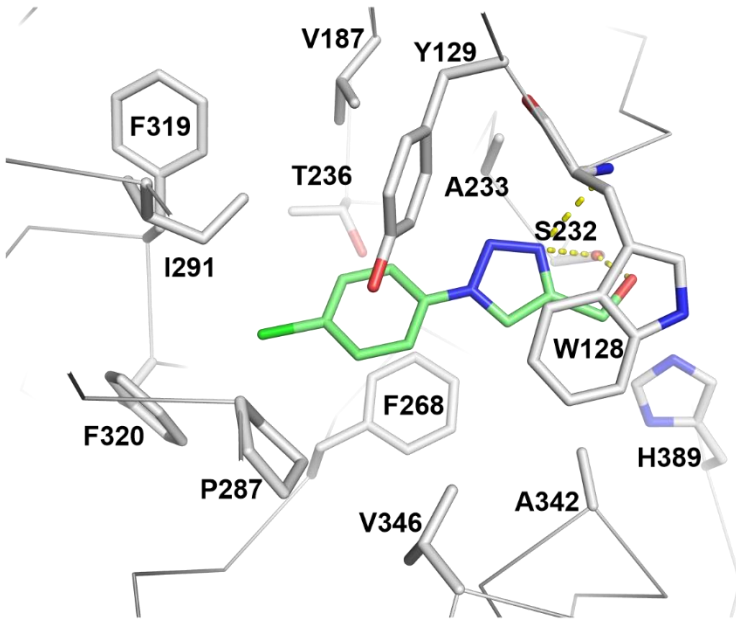
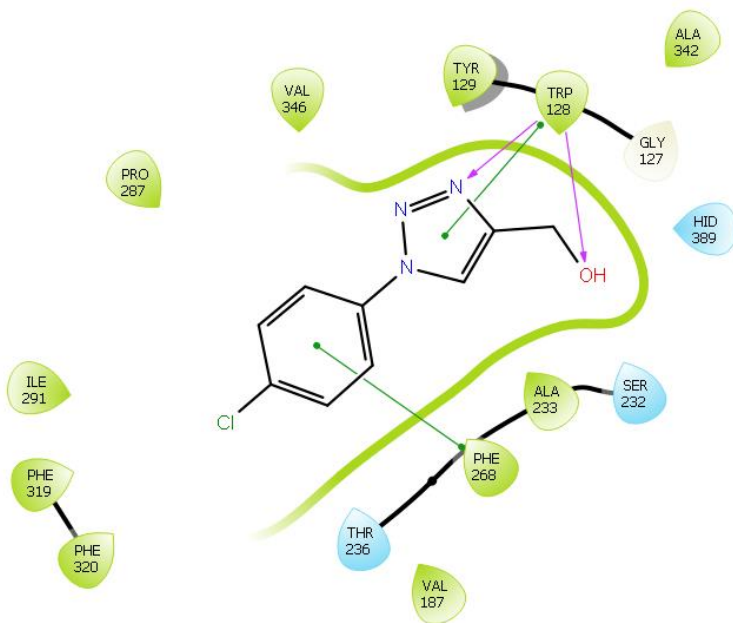
Inhibition of Notum carboxylesterase activity of these hits was measured in a biochemical assay where test compounds (dispensed to give 10-point concentration-response-curves up to 100 μ M) were incubated with human Notum(81-451 Cys330Ser) and trisodium 8-octanoyloxypyrene-1,3,6-trisulfonate (OPTS) as the substrate, and fluorescence recorded; an inhibitor of Notum would suppress fluorescence by binding to Notum and preventing hydrolysis of OPTS.

A standout hit from this set was (1-(4-chlorophenyl)-1*H*-1,2,3-triazol-4-yl)methanol (**7**) (**Figures 2 and 3**). The binding pose of **7**, as identified in the crystal structure, showed occupation of the palmitoleate binding pocket by the *N*-(4-chlorophenyl) substituent, forming a pi-pi stacking interaction with residue Phe268 (**Figure 3B and 3C**). The triazole head group shows possible pi-pi stacking interactions with Trp128 and hydrogen bonding between the triazole N2 and peptidic backbone of Trp128. Residue Trp128 is also involved in a hydrogen bond to the oxygen of the methyl alcohol group. Compared to the crystal structure of *O*-palmitoleoyl serine (**Figure 3D**), compound **7** occupies approximately the same volume of the pocket as the palmitoleic tail. However, the interaction with the oxyanion hole is more pronounced for the carbonyl of the palmitoleic ester with hydrogen bonds to three separate amino acids (Gly127, Trp128, Ala223) rather than just Trp128 as observed with **7**.

Triazole **7** was determined to be a potent inhibitor of Notum carboxylesterase activity, IC_{50} 11.5 ± 3.0 μ M ($n = 4$), with excellent hit-like properties (mw 209; clog*P* 1.5; TPSA 48) and design metrics (LE = 0.49; LLE = 3.4).^{22,23} Furthermore, the N1-phenyl triazole structural motif is highly chemically enabled to support the rapid exploration structure-activity relationships (SAR) through the application of established synthetic methods. These features combined to identify **7** as an attractive starting point for a structure-based drug design (SBDD) hit-to-lead program.

Figure 2. Work flow for the fragment screen and summary of properties for fragment hit **7**.



A**B****C**

D

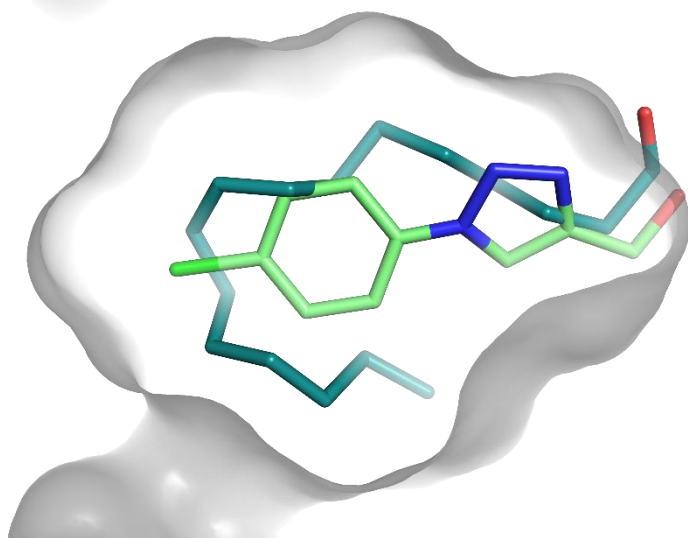


Figure 3: **A:** Electron density $|F_o - F_c|$ omit map. Electron density from Notum complex with **7** (lime) shown as sky blue mesh contoured at 3σ . **B:** Notum-**7** binding details (PDB 6ZUV). Notum residues (gray) interacting with **7** (lime) are defined with distance $<4 \text{ \AA}$. **7** is sandwiched between Phe268 in the back of the pocket and Trp128. The backbone of Trp128 also forms a hydrogen bond with **7** (yellow dashed lines). **C:** Notum-**7** interaction diagram showing all residues within 4 \AA . Pi-stacking interactions (green lines) and hydrogen bonds (purple arrows) are highlighted. **D:** Overlay of **7** (lime) with *O*-palmitoleoyl serine (teal) (PDB 4UZQ) with the surface of the Notum palmitoleoyl binding pocket outlined (gray). Water molecules have been removed for clarity.

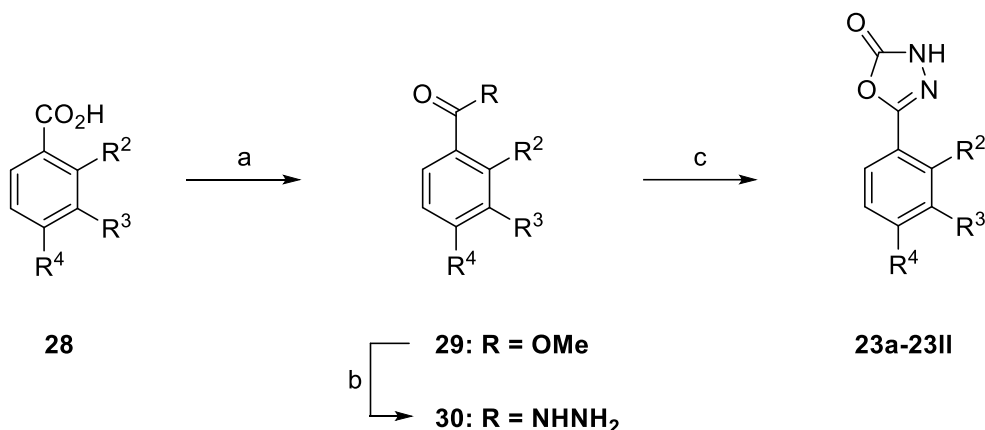
The simple disconnection of hit **7** into its triazole (heterocycle) and 4-chlorophenyl (aryl) motifs guided our general design strategy. New compounds were designed to improve inhibition of Notum activity through modifications at these two principle areas: (1) the heterocycle which sits at the mouth of the pocket near the catalytic triad **8-25** (**Tables 1 and 2**); and (2) the aryl ring that binds in the palmitoleate pocket **23a-23bb** (**Table 3**). Compound design was further guided by the Notum crystal structure and *in silico* docking of design ideas. Additional bespoke modifications of preferred leads were then performed to further improve activity and tune physicochemical properties (mw, clogP, pK_a) to be consistent with good *in vitro* ADME property space (**Table 4**). Selected compounds were screened for aqueous solubility, transit performance in MDCK-MDR1 cell lines for permeability, and metabolic stability in mouse and human liver microsomes (MLM and HLM resp.) to prioritize compounds for *in vivo* studies. Preferred compounds were dosed orally in mouse to determine their pharmacokinetic properties including BBB permeability.

Initially, the effect of modification of the heterocyclic head-group was investigated whilst retaining the pendant hydroxymethyl and the 4-chlorophenyl groups; this single group change would allow the direct comparison of the impact of these azoles **8-15** (**Table 1**). The analogues were either sourced commercially or prepared using established methods. Further substitution by a methyl on the C-5 position of the 1,2,3-triazole **8** (and N-4 of the 1,2,4-triazole **9**) seemed to be disfavored as there was a loss of potency, although these were the only analogues screened to test this hypothesis. It was feasible to replace the 1,2,3-triazole ring with either an oxazole **10**, isoxazole **11** and **12**, or oxadiazoles **13-15** as all showed reasonable activity. A 2- to 3-fold improvement in activity over **7** was achieved with isoxazole **11**, however this was achieved at expense of slightly increased lipophilicity (clogP 1.9, LLE 3.5).

The next phase of SAR investigation was the deletion of the hydroxymethyl group, or truncation to the directly attached hydroxyl, in a series of 4-chlorophenyl heterocycles **16-25** (**Table 2**). The N1 triazole **16** (IC₅₀ 2.9 μM, clogP 2.6) showed an improvement in activity compared to **7**, as did the C4 isomer **17**, and was selected as an early lead for further optimization; full details of this work will be reported separately.²⁴ In contrast, the N1 pyrazole **18** and C5 tetrazole **19** were inferior. The hydroxyl substituted azoles **20-25** gave a broad range in activities (1 μM to >100 μM) and identified weakly acidic 1,3,4-oxadiazol-2(3H)-one **23** as a breakthrough compound due to its improved Notum inhibition activity and physicochemical properties (IC₅₀ 2.1 μM, clogP 2.7). Hence, **23** was selected for further optimization due to these factors and, in part, because of the successful application of oxadiazoles in drug discovery programs.²⁵ In addition, **23** was of interest as a lead to explore the potential of weak acids to penetrate the brain as molecules with these properties are under-represented in CNS drug discovery.^{26,27} 1,2-Isoxazol-3-one **24** and 1,3,4-thiadiazol-2-one **25** also demonstrated

a similar potency to **23**, and the latter heterocycle was revisited once an optimized aryl group had been identified.

At this point in the program, it was encouraging that two complementary leads had been identified from one hit, i.e. triazole **16** and oxadiazole **23** were created from original x-ray fragment screening hit **7**.



Scheme 1. Preparation of 1,3,4-oxadiazol-2(3H)-ones **23**. Representative reagents and conditions: (a) H_2SO_4 (0.5 equiv.), MeOH, RT - 85 °C or SOCl_2 (5 equiv.), MeOH, 0 °C - RT; (b) $\text{N}_2\text{H}_4 \cdot \text{H}_2\text{O}$ (8 equiv.), EtOH-PhMe, 70 °C; (c) Triphosgene (0.4 equiv.), $^i\text{Pr}_2\text{NEt}$ (2 equiv.), CH_2Cl_2 , 0 °C - RT.

With the selection of 1,3,4-oxadiazol-2-one as a preferred heterocycle, we required a reliable synthesis of substituted 5-phenyl-1,3,4-oxadiazol-2-ones for the development of the aryl ring SARs (**Tables 3** and **4**). Target compounds **23a-23II** were readily prepared in three steps from the corresponding benzoic acids **28** (**Scheme 1**). Acids **28** were either purchased or prepared using a customized synthesis, and then esterification with methanol gave methyl esters **29**. Treatment of **29** with excess hydrazine gave the corresponding acylhydrazides **30** which were then cyclized with triphosgene to afford oxadiazolones **23a-23II**.

We first explored the SAR of the aryl ring with variety of single substituents at the *ortho*-, *meta*- and *para*-positions **23a-23bb** (**Table 3**). The unsubstituted phenyl **23a** (IC_{50} 41 μM) was prepared and screened as the benchmark to assess these changes; it is interesting to note that **23a** was ca. 20-fold weaker than the 4-Cl hit **23** and proved to be the weakest compound of all the aryl analogues in **Table 3** showing SAR was tolerant of a variety of groups within this pocket.

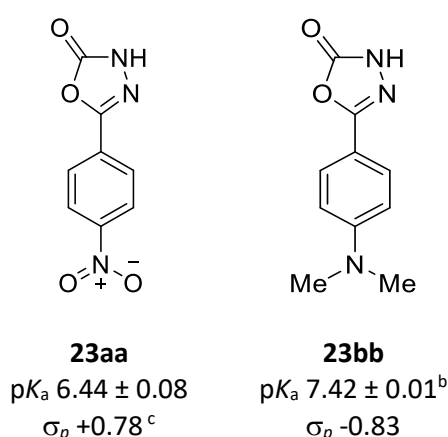
The tactic of walking a Cl, F, Me, and CF_3 around the phenyl ring showed a clear preference for a CF_3 group at all positions (**23e**, **23I**, **23v**) (**Table 3**). A broader range of substituents were then prepared with a bias towards substitution at the *meta*- and *para*-positions. In general, the preferred groups from this exercise were compounds with small lipophilic groups such as Et (**23i**, **23q**), cPr (**23j**, **23r**), CF_3 (**23I**, **23v**), NMe_2 (**23n**, **23bb**),

and OiPr (**23y**) all achieving IC_{50} s $<0.5 \mu\text{M}$. The most potent single substituent Notum inhibitors were 4-iPr (**23s**; IC_{50} $0.075 \mu\text{M}$) and 4-tBu (**23t**; IC_{50} $0.051 \mu\text{M}$). Incorporation of polar substitutions such as 4-CN (**23w**) and 4-NO₂ (**23t**) were detrimental to activity but still superior to having no substituent (cf **23a**).

There emerged a clear trend within this set that inhibition of Notum activity was related to the lipophilicity of the substituent with the most potent compounds having the highest lipophilicity as assessed by $\text{clog}P$ and lipophilic fragmental constants (π) (**Figure S1**). Additionally, modelling suggested that larger substituents were favorable in order to fully occupy the binding pocket.

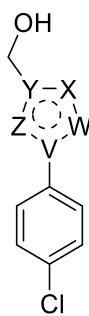
The weakly acidic nature of 5-phenyl-1,3,4-oxadiazole-2(3*H*)-one (**23a**, calculated pK_a ca. 5.8-7.1²⁸) prompted us to consider if it would be feasible to further reduce the acidity of the oxadiazolone head-group to $pK_a > 7.4$ and so increase the fraction of non-ionized drug at physiological pH. A reduction in acidic pK_a would potentially better align the physicochemical properties of this template with CNS drugs as acidic pK_a values for CNS drugs rarely fall below 6.0.^{26,27} From our compound collection, two disparate examples of electron deficient (**23aa**; 4-NO₂) and electron rich (**23bb**; 4-NMe₂) aryl substituents were selected for pK_a measurement (**Figure 4**). This exercise would establish the likely dynamic range of the acidity of N3-H of the 1,3,4-oxadiazol-2(3*H*)-one through the influence of a single substituent at the 4-position of the aryl ring. The results suggested it was reasonable to modulate the pK_a of the 1,3,4-oxadiazolone within a range of one log-unit, and that a strongly electron releasing substituent (4-NMe₂) could reduce the acidic pK_a to 7.4.

Figure 4. Measured acidic pK_a s of *para*-substituted 5-phenyl-1,3,4-oxadiazol-2(3*H*)-ones.^a



^a pK_a of 1,3,4-oxadiazol-2(3*H*)-one reported. ^b pK_a of dimethylamino substituent measured as 2.92 ± 0.06 . ^c Hammett *para*-substituent constant (σ_p).

Table 1: Notum inhibition of 4-chlorophenyl hydroxymethyl azoles **7-15**.^a



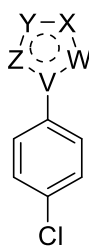
7-15

Compound	7	8	9	10	11	12	13	14	15
Notum IC₅₀ (μM)	11.5 ± 3.0	42 ± 10	>100 ^b	17 ± 5	4.0 ± 0.5	19 ± 4	14 ± 0.3	36 ± 5	65 ± 21

^a All values are mean ± s.d. of n = 2-8 experiments quoted to 2 s.f.

^b 20-30 % I @ 100 μM.

Table 2: Notum inhibition of 4-chlorophenyl azoles **16-25**.^a



16-25

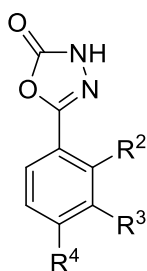
Compound	16	17	18	19
Notum IC₅₀ (μM)	2.9 ± 1.0	4.2 ± 0.2	69 ± 8	>100 ^c

Compound	20	21	22	23	24	25
Notum IC₅₀ (μM)	>100 ^b	77 ± 32	>100 ^b	2.1 ± 0.6	1.6 ± 0.2	0.94 ± 0.03

^a See footnotes Table 1.

^b <20 % I @ 100 μM.

^c 30-50 % I @ 100 μM.

Table 3: Notum inhibition of mono-substituted 5-phenyl-1,3,4-oxadiazol-2(3*H*)-ones **23**.**23a-bb**

Compound	R ² ; R ³ ; R ⁴	Notum IC ₅₀ (μM)
23a	H	41 ± 5
<i>2-substituents (R²)</i>		
23b	2-Cl	6.7 ± 2.7
23c	2-F	11 ± 3
23d	2-Me	3.6 ± 0.2
23e	2-CF ₃	0.43 ± 0.27
<i>3-substituents (R³)</i>		
23f	3-Cl	1.8 ± 0.5
23g	3-F	13 ± 4
23h	3-Me	2.9 ± 0.3
23i	3-Et	0.45 ± 0.25
23j	3-cPr	0.26 ± 0.12
23k	3-CHF ₂	3.1 ± 0.8
23l	3-CF ₃	0.78 ± 0.02
23m	3-OMe	1.2 ± 0.4
23n	3-NMe ₂	0.19 ± 0.09
<i>4-substituents (R⁴)</i>		
23	4-Cl	2.1 ± 0.6
23o	4-F	3.5 ± 0.7
23p	4-Me	2.0 ± 0.6
23q	4-Et	0.27 ± 0.12
23r	4-cPr	0.26 ± 0.08
23s	4-iPr	0.075 ± 0.014
23t	4-tBu	0.051 ± 0.030
23u	4-CHF ₂	3.0 ± 0.5
23v	4-CF ₃	0.46 ± 0.7
23w	4-CN	27 ± 13
23x	4-OMe	1.4 ± 0.2
23y	4-OiPr	0.35 ± 0.20
23aa	4-NO ₂	18 ± 3
23bb	4-NMe ₂	0.19 ± 0.02

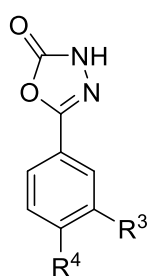
^a See footnotes Table 1.

The application of two substituents at the 3- and 4-positions on the phenyl ring was then explored by building on earlier SAR with a subset of preferred groups (Cl, CF₃, cPr, iPr, NR₂) (**23cc-23ll**; **Table 4**). 3,4-Dichloro **23cc** further improved Notum inhibition activity when compared to the mono-substituted 3-Cl and 4-Cl analogues (**23cc** v **23f** v **23**) which supported this approach. The combination of a 3-CF₃ group with preferred groups at the 4-position gave some of the most potent compounds prepared so far: 3-CF₃-4-Cl (**23dd**; IC₅₀ 18 nM), 3-CF₃-4-iPr (**23ff**; IC₅₀ 6.2 nM), and 3-CF₃-4-cPr (**23gg**; IC₅₀ 1.8 nM). Switching the position of the 3- and 4-substituents of **23gg** gave **23hh** (3-cPr-4-CF₃; IC₅₀ 2.9 nM) which was also a very potent inhibitor of Notum. Evaluation of selected compounds in MLM showed only **23dd** demonstrated high metabolic stability with the potential advantage of low metabolic clearance in vivo. Compound **23dd** also showed high cell permeability in the MDCK-MDR1 assay with a low efflux ratio (ER = 1.6) suggesting minimal recognition by P-gp mediated efflux transport.

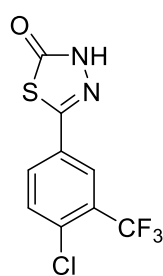
Extending this approach by exploring amino substituents (**23ii**) or amines incorporated into a 3,4-fused ring system (**23jj-II**) identified **23ii** (3-CF₃-4-NMe₂; IC₅₀ 15 nM) as a potent inhibitor of Notum but with poor metabolic stability in MLM. It proved challenging to combine potent Notum inhibition with metabolic stability through the application of substituents designed to reduce the pK_a of the oxadiazolone.²⁴

Revisiting the 1,3,4-thiadiazol-2-one head-group (cf **23** v **25**) in combination with the 3-Cl-4-CF₃ aryl ring gave **26** (IC₅₀ 31 nM) which was also a potent inhibitor of Notum, albeit with inferior metabolic stability. Similarly, 1,3,4-oxadiazole **27** was equipotent to **23dd** but with moderate MLM stability and offered no advantage over **23dd**.

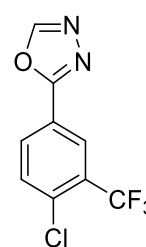
Table 4: Notum inhibition, microsomal stability, cell permeability and aqueous solubility of 1,3,4-oxadiazol-2(3*H*)-ones **23cc-23ll**, 1,3,4-thiadiazol-2(3*H*)-one **26** and 1,3,4-oxadiazole **27**.^{a,b}



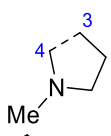
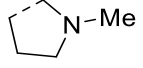
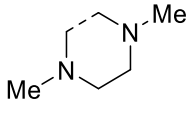
23cc-23ll



26



27

Compound	R ³	R ⁴	Notum IC ₅₀ (nM)	MLM/HLM Cl _i (μL/min/mg)	MDCK-MDR1 AB/BA P _{app} (x10 ⁻⁶ cm/s)	Solubility (μg/mL)/(μM)	LogD _{7.4}
23cc	Cl	Cl	430 ± 80				2.4
23dd	CF ₃	Cl	18 ± 3	<1/1.8	34/55	190/710	2.6
23ee	CF ₃	Me	31 ± 3				
23ff	CF ₃	iPr	6.2 ± 2.3	12/-			
23gg	CF ₃	cPr	1.8 ± 0.4	28/-			
23hh	cPr	CF ₃	2.9 ± 0.3				
23ii	CF ₃	NMe ₂	15 ± 6	96/-			
23jj			380 ± 37				
23kk			33 ± 7				
23ll			32 ± 10				
26	-	-	31 ± 13	26/7.5	45/70	6/22	
27	-	-	13 ± 5	24/-		40/160	

^a See footnotes Table 1.

^b MLM/HLM, MDCK-MDR1 and solubility studies reported in this work were independently performed by GVK Biosciences (Hyderabad, India) or Cyprotex (Macclesfield, UK).

Hence, **23dd** emerged as having a superior profile from this set and was selected for further evaluation as a lead for the program (**Table 5**). Compound **23dd** has physicochemical and molecular properties consistent with small molecule lead-like chemical space (mw 265; clogP 2.9; logD_{7.4} 2.6; TPSA 59.2). The oxadiazole head-group of **23dd** contains a weakly acidic proton at N3 with a measured pK_a 6.7, and so **23dd** would be ca. 85 % ionized at pH 7.4. Assessment of **23dd** by standard design metrics (LE 0.64; LLE 4.8) showed improvement over the original fragment hit **7** and properties consistent with CNS drug-like space²⁹ including a favorable 'CNS multiparameter optimization' score (CNS MPO = 5.7/6.0).³⁰ Additional *in vitro* ADME studies measured binding to mouse plasma proteins (f_u 0.069) and mouse brain tissue (f_u 0.011) showing a preferential binding to brain tissue, and **23dd** did not significantly inhibit representative CYP450 enzymes.

Notum inhibitor **23dd** was screened in a cell-based TCF/LEF reporter gene (Luciferase) assay to assess its ability to restore Wnt/ β -catenin signaling when activated by exogenous rWNT3a (100 ng/mL) in the presence of Notum (500 ng/mL) (**Table 5**).¹⁶ Compound **23dd** showed an activation of Wnt signaling (EC₅₀ ca. 3500 \pm 2200 nM (n = 8)) in this model system through inhibition of Notum in a concentration dependent manner. Performing this experiment in the absence of Notum showed a maximal Wnt response at all concentrations of **23dd** tested (0.3 nM to 10 μ M; (n = 4)) confirming the outcome was due to direct inhibition of Notum activity and not related to assay interference or cell toxicity (up to 10 μ M).

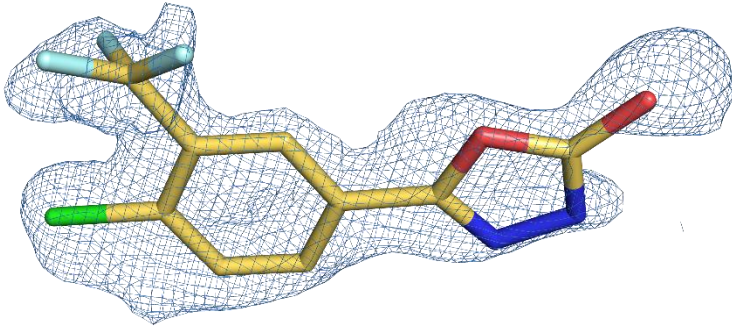
Representative inhibitors were tested in a Notum occupancy assay using FP-biotin, a serine hydrolase activity-based probe, whereby labelling of Notum with FP-biotin can be blocked by an inhibitor occupying the active site of Notum.^{16,31} Inhibitors **23dd** and **27** showed some ability to prevent labelling by FP-biotin, confirming they competitively bind to Notum, albeit with modest potency compared to **1**. While target engagement is demonstrated, this data also shows disparities between different chemotypes with similar activity in the Notum OPTS assay (**Figure S2**).

Table 5. Summary of physicochemical and molecular properties, Notum inhibition and ADME data for **23dd**.^a

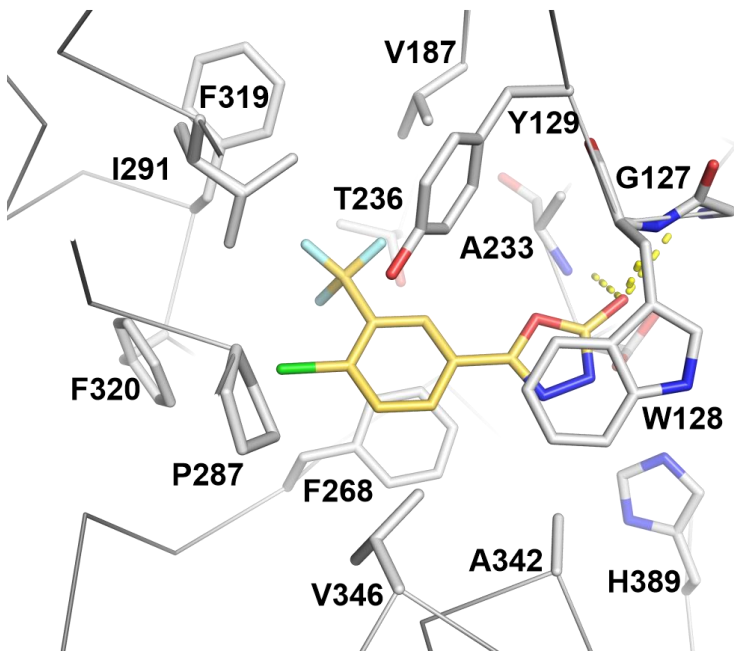
	23dd
<i>Physicochemical and molecular properties</i>	
mol wt	265
clogP	2.9
logD _{7.4}	2.6
TPSA (Å ²)	59.2
CNS MPO	5.7
pK _a	6.7
<i>Notum inhibition</i>	
OPTS, IC ₅₀ (nM)	18 ± 3 (n = 8)
TCF-LEF, EC ₅₀ (nM)	3500 ± 2200 (n = 8)
<i>ADME profile</i>	
Aq. solubility (μg/mL)/(μM)	188/710
Mouse plasma protein binding (PPB) (%)	93.1
Mouse brain binding (%)	98.9
MLM, Cl _i (μL/min/mg protein)	0.42
CYP1A2 inhibition, IC ₅₀ (μM)	16.6
CYP2C9 inhibition, IC ₅₀ (μM)	>25
CYP2C19 inhibition, IC ₅₀ (μM)	>25
CYP2D6 inhibition, IC ₅₀ (μM)	>25
CYP3A4 inhibition, IC ₅₀ (μM)	>25
MDCK-MDR1, AB/BA <i>P</i> _{app} (x10 ⁻⁶ cm/s)	34/55
MDCK-MDR1, Efflux ratio (ER)	1.64

^a See footnotes Table 4, and Figure S3.

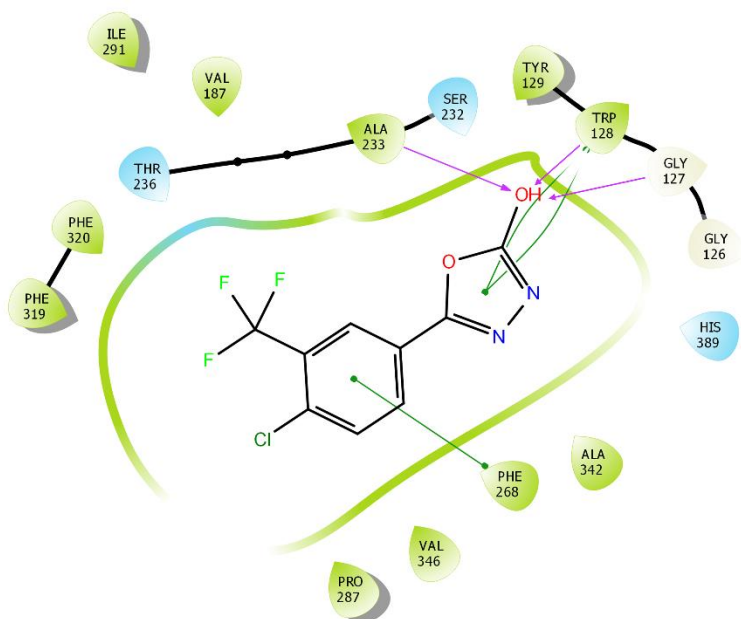
A



B



C



D

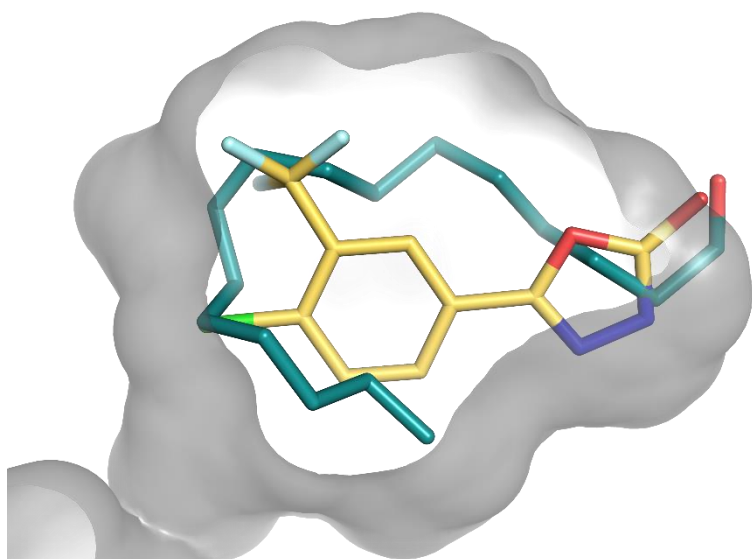


Figure 5: **A:** Electron density $|F_o - F_c|$ omit map. Electron density from Notum complex with **23dd** (gold) shown as sky blue mesh contoured at 3σ . **B:** Notum-**23dd** binding details (PDB 6ZVL). Notum residues (gray) interacting with **23dd** (gold) are defined with distance $<4 \text{ \AA}$. Note I291 and S232 show alternative conformations. **C:** Notum-**23dd** interaction diagram showing all residues within 4 \AA . Pi-stacking interactions (green lines) and hydrogen bonds (purple arrows) are highlighted. **D:** Overlay of **23dd** (gold) with *O*-palmitoleoyl serine (teal) (PDB 4UZQ) with the surface of the Notum palmitoleoyl binding pocket outlined (grey). Water molecules have been removed for clarity.

The binding mode of **23dd** is shown in **Figure 5**. In contrast to the original fragment hit **7 (Figure 3)**, **23dd** is making a complete interaction with the oxyanion hole similar to the palmitoleic ester while occupying an increased volume of the palmitoleate hydrophobic pocket.

Modelling the inhibitors **23a-23ll** in the active site of Notum by molecular docking using the crystal structure of **23dd** reveal that the more potent inhibitors tend to occupy the pocket more completely with substituents also filling the back of this pocket as can be clearly seen for **23dd** in **Figure 5**. Due to the highly lipophilic nature of the palmitoleate pocket, the preferred groups accepted also tend to be highly lipophilic.

Table 6. Mouse pharmacokinetic data for **23dd**; oral (p.o.) dose at 10 mg/kg.^a

PK Parameter	23dd	
	Plasma	Brain
T _{1/2}	3.7 h	2.3 h
T _{max}	0.5 h	0.17 h
C _{max}	16600 ng/mL	2990 ng/g
AUC _(0→t)	50400 ng.h/mL	8870 ng.h/g
AUC _(0→inf)	63100 ng.h/mL	9910 ng.h/g
K _p ^b		0.16
K _{p,uu} ^c		0.025

^a Male C57BL6 mice; suspension formulation in 0.1% Tween80 in water; n = 3 per time point; terminal blood and brain levels measured at 0.17, 0.50, 1, 2, 4, 8 and 24 h. All animals were healthy throughout the study period. ^b The brain-to-plasma ratio (K_p) was calculated by the ratio of AUC_(0→inf) of brain concentration-time profile (AUC_{(0→inf), brain}) to that of plasma concentration-time profile (AUC_{(0→inf), plasma}). ^c Free partition coefficient of brain (K_{p,uu}) was calculated by multiplying the K_p with the ratio of free fraction in brain homogenate to plasma (f_{u,brain}/f_{u,plasma}).

Pharmacokinetic data for **23dd** was generated *in vivo* in mouse to evaluate plasma exposure and BBB penetration (**Table 6; Figure S4**). Following single oral dose (p.o.) of 10 mg/kg, plasma exposure achieved a C_{max}[plasma] ≈ 4.3 μM (free drug) with rapid absorption. Compound **23dd** demonstrated modest BBB penetration with a brain-to-plasma concentration ratio of 0.16 based on AUC_(0→inf) (total drug, K_p), which was reduced to 0.025 (free drug, K_{p,uu}) when unbound drug levels in brain and plasma were used. The combination of incomplete BBB penetration along with preferential binding to brain tissue resulted in moderate brain exposure of C_{max} [brain] ≈ 0.12 μM (free drug) from this dose.

The plasma half-life and terminal clearance of **23dd** were consistent with the microsomal stability data in MLM. However, the partial BBB penetration was somewhat unexpected based on the design criteria, *in silico* and cell models employed leading to the *in vivo* assessment. The BBB provides protection to the CNS from exposure to circulating chemicals by maintaining tight junctions between endothelial cells and through range of transporter proteins that regulate exchange between blood and the CNS. The ABC transporters are generally regarded as the most important transporters that restrict the permeability of toxins and therapeutic agents across the BBB with the P-gp, BCRP, and MRP efflux transporters having significant roles.³² These ABC transporters are able to recognize and efflux a diverse range of drugs and have, in part, overlapping substrates belonging to different chemical classes.

The reason for the partial BBB exposure of **23dd** will not be simple to establish due to the complex nature of the BBB and the multiple parameters that influence BBB permeability. Although **23dd** seems to have physicochemical properties entirely consistent with *passive* BBB permeability²⁹ and excellent permeability as measured by transit performance in MDCK-MDR1 cell lines without evidence for P-gp recognition and efflux, **23dd** may prove to be a substrate for other BBB efflux transporters.³² P-gp substrates are usually lipophilic and either neutral or cationic, whereas MRPs prefer anionic substrates and BCRP transports both cations and anions. As **23dd** is weakly acidic and would be predominantly anionic at physiological pH, we propose that it may be a substrate for the MRP or BCRP efflux transporters.

The apparent disconnection between these *in vitro* and *in vivo* models also recommends the early assessment of a chemical tool in rodent PK experiments to establish a correlation (or otherwise) between the predictive models employed and *in vivo* outcomes for BBB permeability.

In summary, the mouse PK experiments support the use of **23dd** as a new chemical tool for exploring the role of Notum mediated regulation of Wnt signaling for peripheral disease. However, its incomplete BBB penetration and modest free drug levels in the brain at these doses mean **23dd** is probably not suitable for use in animal models of CNS disease. Recent efforts have identified amide **2**¹⁴ and oxadiazole **23dd** (this work) both with partial BBB permeability (**Table S2**). Hence, there is still the need for an improved inhibitor of Notum activity for use as a chemical probe to investigate the regulation of Wnt signaling in the CNS and demonstrate modulation of AD phenotypes in mouse models.

We propose **23dd** represents a quality addition to the small molecule ‘toolbox’ of Notum inhibitors as it is a new chemotype with a complementary profile to **1-3**.

CONCLUSION

A crystallographic x-ray fragment screen with carboxylesterase Notum identified (1-(4-chlorophenyl)-1*H*-1,2,3-triazol-4-yl)methanol (**7**) as an attractive starting point for a SBDD hit-to-lead program. Optimization of fragment hit **7** (IC₅₀ 11.5 μM) by SAR of the heterocyclic head-group identified two early lead series as potent inhibitors of Notum activity: triazole **16** (IC₅₀ 2.9 μM) and oxadiazole **23** (IC₅₀ 2.1 μM). Further investigation of the oxadiazole series **23** by exploring substitution on the aryl ring which binds deep in the palmitoleate pocket identified **23dd** as a preferred example.

Compound **23dd** has physicochemical properties consistent with drug-like chemical space and contains a weakly acidic proton with a measured pK_a 6.7. Compound **23dd** demonstrated good metabolic stability in MLM and HLM, and cell permeability in the MDCK-MDR1 assay with no evidence for P-gp mediated efflux. Compound **23dd** restored Wnt/β-catenin signaling in a cell-based TCF/LEF reporter gene assay when activated by exogenous rWNT3a in the presence of Notum. PK studies with **23dd** were performed *in vivo* in mouse with single oral administration of **23dd** showing good plasma exposure but partial BBB penetration.

An x-ray crystallographic structure determined the binding mode of **23dd** in Notum. Inhibitor **23dd** makes an effective interaction with the oxyanion hole with hydrogen bonds to three separate amino acids (Gly127, Trp128, Ala223) while still filling the hydrophobic palmitoleate pocket.

Significant progress was made in developing x-ray fragment hit **7** into lead **23dd** (>600-fold increase in activity) which showed good plasma exposure in mouse PK experiments making it suitable as a new chemical tool for exploring the role of Notum mediated regulation of Wnt signaling for non-CNS disease. Furthermore, contemporaneous studies with alternative lead triazole **16** identified ARUK3001185, which was shown to be a potent, selective and CNS penetrant inhibitor of Notum activity suitable for use in both cellular and *in vivo* models of CNS disease.²⁴ Full details of this research will be published in due course.

EXPERIMENTAL SECTION

Chemistry

General Information:

Unless preparative details are provided, all reagents were purchased from commercial suppliers and used without further purification. Solvents were of ACS reagent grade or higher and purchased from commercial suppliers without further purification. Anhydrous solvents were purchased as such from Acros Organics or Sigma Aldrich. Thin layer chromatography (TLC) was carried out on aluminum backed silica plates. The plates were visualized under UV (254 nm) light, followed by staining with phosphomolybdic acid dip or potassium permanganate and gentle heating.

COware gas reactor (total volume 100 mL) was purchased from Sigma-Aldrich (catalogue number STW5).

Compound purification by column chromatography was performed using a Biotage Isolera using prepacked Biotage SNAP KP-Sil silica cartridges or Biotage SNAP Ultra C18 reverse phase cartridges. Organic solvent layers were routinely dried with anhydrous MgSO₄ and concentrated using a Büchi rotary evaporator.

Melting points (mp) were determined using Stuart SMP20 melting point equipment using closed end glass capillary tubes and are uncorrected.

Infra-red (IR) spectra were recorded on a Shimadzu IRTracer-100 FT-IR spectrometer, using a Universal ATR accessory for sampling, with relevant absorbance quoted as ν_{\max} in cm⁻¹.

¹H NMR and ¹³C NMR spectra were run in deuterated (≥99.5%) solvents on either a Bruker Avance 300 (300 MHz), Bruker Avance 400 (400 MHz), Bruker Avance 600 (600 MHz) or Bruker Avance 700 (700 MHz). Chemical shifts (δ) are reported as parts per million (ppm), coupling constants (*J*) are reported in Hz and signal multiplicities are reported as singlet (s), doublet (d), triplet (t), quartet (q), pentet (p), quintet (qu), sextet (sext), doublet of doublets (dd), doublet of triplets (dt), triplet of triplets (tt), multiplet (m), or broad singlet (br s).

LCMS analysis was performed on a Waters Acquity H-Class UPLC system with either an acidic (HSS C18 Column, H₂O:MeCN, 0.1% TFA) or basic (BEH C18 Column, H₂O:MeCN, 10 mM NH₄OH) mobile phase.

HRMS data acquisition was on a Waters Micromass LCT Premier electrospray time-of-flight (ESI-TOF) mass spectrometer. The observed mass and isotope pattern matched the corresponding theoretical values as calculated from the expected elemental formula.

Purity of screening compounds **7-27** was evaluated by NMR spectroscopy and LCMS analysis. All compounds had purity ≥95 % unless otherwise stated.

General Methods:

1. Preparation of methyl esters **29**.

1.1 Sulfuric acid catalysed.

Sulfuric acid (60 μ L, 1.11 mmol, 0.5 equiv.) was added to a solution of carboxylic acid **28** (2.23 mmol, 1.0 equiv.) in MeOH (10 mL) and heated to 85 °C for 3 d. The reaction mixture was then cooled to RT, concentrated to approximately one third volume, then diluted with EtOAc and saturated aqueous NaHCO₃. The organic phase was dried, filtered and concentrated under reduced pressure to give the ester **29**, which was used without further purification.

1.2 Thionyl chloride promoted.

Thionyl chloride (0.83 mL, 7.26 mmol, 5.0 equiv.), was added dropwise to a solution of carboxylic acid **28** (1.45 mmol, 1.0 equiv.) in MeOH (8 mL) at 0 °C (external). The reaction mixture was heated to reflux for 2 h, cooled to RT and concentrated under reduced pressure. The residue was then passed through a short pad of silica (0-20% EtOAc in cyclohexane) to provide ester **29**, which was used without further purification.

1.3 (Trimethylsilyl)diazomethane promoted.

A solution of (trimethylsilyl)diazomethane (1.13 mL, 2 M in hexanes, 2.27 mmol, 1.05 equiv.) was added dropwise to a precooled solution of carboxylic acid **28** (2.16 mmol, 1.0 equiv.) in MeOH at 0 °C (external) (upon addition, mild bubbling is observed). Following complete addition, the reaction mixture remained a faint yellow colour. Acetic acid was added dropwise until the reaction mixture turned colourless (complete consumption of the excess TMSCH₂N₂). The reaction mixture was concentrated under reduced pressure to give the ester **29**, which was used without further purification.

2. Preparation of acyl hydrazides **30**.

Hydrazine monohydrate (350 mg, 7.0 mmol, 4.0 equiv.) was added to a solution of methyl ester **29** (1.75 mmol) in EtOH (4 mL) and toluene (2 mL). The mixture was heated at 40 °C for 16 h, cooled to RT and then concentrated under reduced pressure. The residue was azeotroped with EtOH and toluene to provide crude acyl hydrazide **30**, which was used without further purification.

A few reactions were performed at higher temperatures (45 to 120 °C) and/or with additional equivalents of hydrazine (8 to 15 equiv.); these modified conditions are presented for each compound as necessary.

3. Preparation of 1,3,4-oxadiazol-2(3H)-ones **23b-23ll**.

A solution of triphosgene (172 mg, 0.58 mmol, 0.4 equiv.) in CH₂Cl₂ (15 mL) was added dropwise to a solution of acyl hydrazide **30** and iPr₂NEt (0.51 mL, 2.9 mmol, 2.0 equiv.) in CH₂Cl₂ (5 mL) at 0 °C (external). The reaction was stirred at 0 °C for 20 min, warmed to RT and stirred for a further 40 min. The reaction mixture was diluted with CH₂Cl₂, and cautiously diluted with saturated aqueous NaHCO₃. The organic phase was dried, filtered and concentrated under reduced pressure. The crude product was purified by column chromatography (0-2 % MeOH in CH₂Cl₂) to give oxadiazolone **23b-23II**.

4. Preparation of 1,3,4-thiadiazol-2(3H)-ones **25** and **26**.

Lawesson's reagent (360 mg, 0.88 mmol, 1.0 equiv.) was suspended in PhMe (5 mL), benzohydrazide **30** (0.88 mmol) was added and the mixture was heated at 110 °C for 16 h. The reaction mixture was quenched by the addition of H₂O (5 mL) and stirring at 50 °C for 10 min. The biphasic mixture was then concentrated under reduced pressure. The residue was purified by reverse phase chromatography (0-100 % MeCN in H₂O, 0.1 % formic acid modifier) to give the benzothiohydrazide which was used immediately in the next step without further purification.

A solution of triphosgene (52 mg, 0.18 mmol) in CH₂Cl₂ (10 mL) was added dropwise to a stirred solution of benzothiohydrazide and iPr₂NEt (0.18 mL, 1.06 mmol) in CH₂Cl₂ (10 mL) at 0 °C (external). The mixture warmed to RT and stirred for 10 min. The reaction was quenched by the addition of saturated aqueous NaHCO₃ and the organic phase was separated and concentrated under pressure. The residue was purified by reverse phase chromatography (0-100 %, MeCN in H₂O, 0.1% NH₄OH modifier) to give the 1,3,4-thiadiazol-2(3H)-one.

Notum inhibitors:

(1-(4-Chlorophenyl)-1H-1,2,3-triazol-4-yl)methanol (7)

Purchased from Key Organics, 4F-329S.

(1-(4-Chlorophenyl)-5-methyl-1H-1,2,3-triazol-4-yl)methanol (8)

Purchased from Key Organics, BS-4321.

[5-(4-Chlorophenyl)-4-methyl-1,2,4-triazol-3-yl]methanol (9)

Purchased from Enamine, EN300-137908.

[5-(4-Chlorophenyl)oxazol-2-yl]methanol (10)

Purchased from Enamine, EN300-263328.

(5-(4-Chlorophenyl)isoxazol-3-yl)methanol (11)

Purchased from Key Organics, 5N-601S.

(3-(4-chlorophenyl)isoxazol-5-yl)methanol (12)

Purchased from Key Organics, 10L-365S.

(5-(4-Chlorophenyl)-1,3,4-oxadiazol-2-yl)methanol (13)

Purchased from Enamine, EN300-65731.

[5-(4-Chlorophenyl)-1,2,4-oxadiazol-3-yl]methanol (14)

Purchased from Enamine, EN300-105946.

(3-(4-Chlorophenyl)-1,2,4-oxadiazol-5-yl)methanol (15)

Purchased from Key Organics, 11X-0223.

1-(4-Chlorophenyl)-1H-1,2,3-triazole (16)

Step 1: Sodium nitrite (144 mg, 2.1 mmol) was added portionwise to a solution of 4-chloroaniline (220 mg, 1.7 mmol) in TFA (3 mL, 3.5 mmol) at 0 °C over 30 min. The reaction mixture was then allowed to warm to RT for 1.5 h, H₂O (0.3 mL) was added and the mixture was re-cooled to 0 °C. Sodium azide (125 mg, 1.9 mmol) was added portionwise over 30 min and the reaction mixture was warmed to RT over 16 h. The mixture was basified to pH 8-9 by the dropwise addition of saturated aqueous NaHCO₃ and extracted with CH₂Cl₂ (2 x 30 mL). The combined organic phase was diluted with *t*-BuOH (2 mL) and the CH₂Cl₂ was cautiously evaporated under reduced pressure at 25 °C to provide a solution of crude 1-azido-4-chlorobenzene, which was used without further purification.

Step 2: MeOH (1 mL), H₂O (2 mL), sodium L-ascorbate (138 mg, 0.7 mmol) and trimethylsilylacetylene (171 mg, 1.7 mmol) were added to the solution of crude azide from Step 1. The reaction mixture was stirred at 50 °C for 16 h, cooled to RT, diluted with brine (10 mL) and extracted with CH₂Cl₂ (2 x 50 mL). The combined organics were dried, concentrated under reduced pressure and the crude product was purified by reverse phase chromatography (0-100 % MeCN in H₂O, 0.1% formic acid modifier) to give **16** (46 mg, 15 %) as a tan solid.

¹H NMR (700 MHz, DMSO-*d*₆) δ 8.86 (d, *J* = 1.2 Hz, 1H), 7.99 (d, *J* = 1.2 Hz, 1H), 7.98 – 7.94 (m, 2H), 7.71 – 7.66 (m, 2H); ¹³C NMR (176 MHz, DMSO-*d*₆) δ 135.5, 134.6, 132.9, 129.9, 123.3, 121.8; LCMS *m/z* 180.0 [M+H]⁺.

4-(4-Chlorophenyl)-2H-1,2,3-triazole (17)

Copper (I) iodide (11 mg, 0.05 mmol, 0.045 equiv.) and 1-chloro-4-ethynylbenzene (150 mg, 1.1 mmol) were dissolved in anhydrous DMF (3 mL) and MeOH (1.5 mL) under an atmosphere of N₂. Azidotrimethylsilane (0.22 mL, 1.65 mmol, 1.5 equiv.) was added dropwise at RT and the reaction was heated to 100 °C for 15 h. The cooled solution was diluted with MeOH and EtOAc, and then concentrated under reduced pressure. The crude product was purified by column chromatography (0-10 % MeOH in CH₂Cl₂) to give **17** (55 mg, 28 %) as a white solid.

¹H NMR (700 MHz, DMSO-*d*₆) δ 15.69-14.82 (m, 1H), 8.75-8.18 (m, 1H), 7.88 (d, *J* = 8.1 Hz, 2H), 7.51 (d, *J* = 8.2 Hz, 2H); LCMS *m/z* 180.1 [M+H]⁺.

1-(4-Chlorophenyl)-1H-pyrazole (18)

Purchased from Key Organics, AS-5194.

5-(4-Chlorophenyl)-2H-tetrazole (19)

Purchased from Sigma Aldrich, CH6371382779.

3-(4-Chlorophenyl)-1-methyl-1H-pyrazol-5-ol (20)

Purchased from Fluorochem, 317356.

3-(4-Chlorophenyl)isoxazol-5-ol (21)

Purchased from Activate Scientific, AS93646.

3-(4-Chlorophenyl)-1,2,4-oxadiazol-5(4H)-one (22)

Methyl chloroformate (0.11 mL, 1.47 mmol) was added dropwise to a suspension of 4-chloro-*N*-hydroxybenzamidine (250 mg, 1.47 mmol) and K₂CO₃ (200 mg, 1.47 mmol) at RT. The mixture was heated to 60 °C for 5 h, cooled to RT, concentrated under reduced pressure, and then purified by reverse phase chromatography (0-100 % MeCN in H₂O, 0.1% formic acid modifier) to give **22** (15 mg, 5 %) as a white solid.

¹H NMR (600 MHz, DMSO-*d*₆) δ 7.79–7.74 (m, 2H), 7.46–7.40 (m, 2H); LCMS *m/z* 195.0 [M-H]⁻.

5-(4-Chlorophenyl)-1,3,4-oxadiazol-2(3H)-one (23)

Purchased from Sigma Aldrich, JRD0393.

5-Phenyl-1,3,4-oxadiazol-2(3H)-one (23a)

Purchased from Key Organics, LE-0723.

5-(2-Chlorophenyl)-1,3,4-oxadiazol-2(3H)-one (23b)

Prepared by General Method 3 from 2-chlorobenzohydrazide. Isolated as a white solid (84 mg, 73 %).

^1H NMR (400 MHz, CDCl_3) δ 9.11 (br s, 1H), 7.82 (dd, $J = 7.9, 1.8$ Hz, 1H), 7.54 (dd, $J = 7.9, 1.4$ Hz, 1H), 7.46 (apparent td, $J = 7.6, 1.8$ Hz, 1H), 7.40 (apparent ftd, $J = 7.6, 1.4$ Hz, 1H); ^{13}C NMR (175 MHz, CDCl_3) δ 154.0, 153.6, 132.8, 132.5, 131.6, 130.2, 127.2, 122.6; LCMS m/z 197.1 $[\text{M}+\text{H}]^+$.

5-(2-Fluorophenyl)-1,3,4-oxadiazol-2(3H)-one (23c)

Prepared by General Method 3 from 2-fluorobenzohydrazide. Isolated as a white solid (74 mg, 84 %).

^1H NMR (600 MHz, $\text{DMSO}-d_6$) δ 12.71 (s, 1H), 7.81 (apparent td, $J = 7.6, 1.7$ Hz, 1H), 7.63 (dddd, $J = 8.4, 7.2, 5.1, 1.8$ Hz, 1H), 7.43 (ddd, $J = 11.2, 8.4, 0.9$ Hz, 1H), 7.38 (apparent td, $J = 7.7, 1.1$ Hz, 1H); ^{13}C NMR (176 MHz, DMSO) δ 159.0 (d, $J = 256.1$ Hz), 154.1, 150.5 (d, $J = 5.0$ Hz), 133.5 (d, $J = 8.5$ Hz), 128.5, 125.1 (d, $J = 3.5$ Hz), 117.0 (d, $J = 20.3$ Hz), 112.2 (d, $J = 11.0$ Hz); LCMS m/z 179.1 $[\text{M}-\text{H}]^-$.

5-(2-Methylphenyl)-1,3,4-oxadiazol-2(3H)-one (23d)

Purchased from Combi-Blocks, WZ-9510.

5-(2-(Trifluoromethyl)phenyl)-1,3,4-oxadiazol-2(3H)-one (23e)

Prepared by General Method 3 from 2-(trifluoromethyl)benzohydrazide. Isolated as a white solid (92 mg, 82 %).

^1H NMR (400 MHz, $\text{DMSO}-d_6$) δ 12.85 (s, 1H), 7.99 – 7.93 (m, 2H), 7.90 – 7.80 (m, 2H); ^{13}C NMR (176 MHz, DMSO) δ 154.4, 151.9, 133.2, 132.1, 131.2, 127.1 (q, $J = 5.4$ Hz), 126.90 (q, $J = 31.8$ Hz), 123.2 (q, $J = 273.5$ Hz), 122.1 (d, $J = 1.7$ Hz); LCMS m/z 229.1 $[\text{M}-\text{H}]^-$.

5-(3-Chlorophenyl)-1,3,4-oxadiazol-2(3H)-one (23f)

Prepared by General Method 3 from 3-chlorobenzohydrazide. Isolated as a white solid (121 mg, 35 %).

^1H NMR (600 MHz, $\text{DMSO}-d_6$) δ 12.93 – 12.45 (m, 1H), 7.77 – 7.73 (m, 2H), 7.65 – 7.63 (m, 1H), 7.59 – 7.56 (m, 1H); ^{13}C NMR (151 MHz, $\text{DMSO}-d_6$) δ 154.3, 152.6, 133.9, 131.3, 131.2, 126.0, 124.7, 123.9; LCMS m/z 195.0 $[\text{M}-\text{H}]^-$.

5-(3-Fluorophenyl)-1,3,4-oxadiazol-2(3H)-one (23g)

Prepared by General Method 3 from 3-fluorobenzohydrazide. Isolated as a white solid (179 mg, 77 %).

^1H NMR (400 MHz, $\text{DMSO}-d_6$) δ 12.72 (s, 1H), 7.67 – 7.54 (m, 3H), 7.47 – 7.39 (m, 1H); ^{13}C NMR (176 MHz, $\text{DMSO}-d_6$) δ 162.2 (d, $J = 245.1$ Hz), 154.3, 152.8 (d, $J = 3.5$ Hz), 131.6 (d, $J = 8.4$ Hz), 126.1 (d, $J = 8.8$ Hz), 121.5 (d, $J = 2.9$ Hz), 118.4 (d, $J = 21.2$ Hz), 112.0 (d, $J = 24.4$ Hz); LCMS m/z 179.1 $[\text{M}-\text{H}]^-$.

5-(3-Methylphenyl)-1,3,4-oxadiazol-2(3H)-one (23h)

Purchased from Combi-Blocks, WZ-9533.

5-(3-Ethylphenyl)-1,3,4-oxadiazol-2(3H)-one (23i)

Prepared by General Methods 1.1, 2 and 3 from 3-ethylbenzoic acid. Isolated as an off-white solid (186 mg, 59 %).

^1H NMR (600 MHz, DMSO- d_6) δ 12.56 (s, 1H), 7.65 – 7.59 (m, 2H), 7.48 – 7.41 (m, 2H), 2.68 (q, J = 7.6 Hz, 2H), 1.20 (t, J = 7.6 Hz, 3H); ^{13}C NMR (151 MHz, DMSO- d_6) δ 154.5, 153.9, 144.9, 131.0, 129.3, 124.4, 124.0, 122.7, 27.9, 15.4; LCMS m/z no parent mass ion detected.

5-(3-Cyclopropylphenyl)-1,3,4-oxadiazol-2(3H)-one (23j)

Prepared by General Methods 1.2, 2 (8 equiv. at 70 °C) and 3 from 3-cyclopropylbenzoic acid. Isolated as a white solid (160 mg, 30 %).

^1H NMR (600 MHz, DMSO) δ 12.56 (s, 1H), 7.58–7.52 (m, 1H), 7.48 (apparent t, J = 1.7 Hz, 1H), 7.41 (apparent t, J = 7.8 Hz, 1H), 7.29–7.24 (m, 1H), 2.03 (apparent tt, J = 8.4, 5.1 Hz, 1H), 1.05–0.95 (m, 2H), 0.77–0.68 (m, 2H); ^{13}C NMR (176 MHz, DMSO) δ 154.5, 153.9, 145.0, 129.2, 128.3, 123.9, 122.3, 122.1, 14.9, 9.7; LCMS m/z 201.1 [M+H] $^+$.

5-(3-(Difluoromethyl)phenyl)-1,3,4-oxadiazol-2(3H)-one (23k)

Prepared by General Methods 1.1, 2 and 3 from 3-(difluoromethyl)benzoic acid. Isolated as an off-white solid (91 mg, 15 %).

^1H NMR (600 MHz, DMSO- d_6) δ 12.70 (s, 1H), 7.99-7.92 (m, 2H), 7.77 (d, J = 7.6 Hz, 1H), 7.71 (apparent t, J = 7.9 Hz, 1H), 7.15 (t, J = 55.6 Hz, 1H); ^{13}C NMR (151 MHz, DMSO- d_6) δ 154.4, 153.1, 135.1 (t, J = 22.4 Hz), 130.1, 128.4, 127.7, 124.7, 122.5, 114.3 (t, J = 236.2 Hz); LCMS m/z 211.1 [M-H] $^-$.

5-(3-(Trifluoromethyl)phenyl)-1,3,4-oxadiazol-2(3H)-one (23l)

Purchased from Combi-Blocks, WZ-9561.

5-(3-Methoxyphenyl)-1,3,4-oxadiazol-2(3H)-one (23m)

Prepared by General Method 3 from 3-methoxybenzohydrazide. Isolated as a white solid (204 mg, 82 %).

^1H NMR (400 MHz, DMSO- d_6) δ 12.61 (s, 1H), 7.46 (apparent t, J = 8.0 Hz, 1H), 7.39–7.33 (m, 1H), 7.26 (dd, J = 2.5, 1.6 Hz, 1H), 7.14 (ddd, J = 8.3, 2.6, 1.0 Hz, 1H), 3.82 (s, 3H); ^{13}C NMR (176 MHz, DMSO- d_6) δ 159.5, 154.4, 153.6, 130.5, 125.2, 117.5, 117.5, 109.9, 55.3; LCMS m/z no mass ion detected.

5-(3-(Dimethylamino)phenyl)-1,3,4-oxadiazol-2(3H)-one (23n)

Prepared by General Method 3 from 3-(dimethylamino)benzohydrazide. Isolated as a white solid (81 mg, 71 %).

^1H NMR (600 MHz, CDCl_3) δ 9.07 (br s, 1H), 7.31 (apparent t, $J = 8.3$ Hz, 1H), 7.19 (apparent dt, $J = 7.7, 1.3$ Hz, 1H), 7.14 (dd, $J = 2.7, 1.3$ Hz, 1H), 6.85 (dd, $J = 8.3, 2.7$ Hz, 1H), 3.00 (s, 6H); ^{13}C NMR (151 MHz, CDCl_3) δ 156.2, 154.9, 150.7, 129.8, 124.5, 115.7, 113.9, 109.1, 40.6; LCMS m/z 206.1 $[\text{M}+\text{H}]^+$.

5-(4-Fluorophenyl)-1,3,4-oxadiazol-2(3H)-one (23o)

Prepared by General Method 3 from 4-fluorobenzohydrazide. Isolated as a white solid (32 mg, 10 %).

^1H NMR (600 MHz, $\text{DMSO}-d_6$) δ 12.58 (s, 1H), 7.89–7.80 (m, 2H), 7.44–7.34 (m, 2H); ^{13}C NMR (151 MHz, $\text{DMSO}-d_6$) δ 163.8 (d, $J = 249.5$ Hz), 154.5, 153.1, 128.0 (d, $J = 9.2$ Hz), 120.7, 116.5 (d, $J = 22.3$ Hz); LCMS m/z 179.1 $[\text{M}-\text{H}]^-$.

5-(4-Methylphenyl)-1,3,4-oxadiazol-2(3H)-one (23p)

Purchased from Key Organics, LE-0722.

5-(4-Ethylphenyl)-1,3,4-oxadiazol-2(3H)-one (23q)

Prepared by General Method 3 from 4-ethylbenzohydrazide. Isolated as a white solid (191 mg, 82 %).

^1H NMR (600 MHz, $\text{DMSO}-d_6$) δ 12.51 (s, 1H), 7.75–7.64 (m, 2H), 7.38 (d, $J = 8.4$ Hz, 2H), 2.67 (q, $J = 7.6$ Hz, 2H), 1.20 (t, $J = 7.6$ Hz, 3H); ^{13}C NMR (176 MHz, $\text{DMSO}-d_6$) δ 154.5, 153.9, 147.6, 128.6, 125.3, 121.5, 28.1, 15.2; LCMS m/z 189.1 $[\text{M}-\text{H}]^-$.

5-(4-Cyclopropylphenyl)-1,3,4-oxadiazol-2(3H)-one (23r)

Prepared by General Methods 1.3, 2 (8 equiv. at 70 °C) and 3 from 4-cyclopropylbenzoic acid. Isolated as a white solid (193 mg, 44 %).

^1H NMR (400 MHz, $\text{DMSO}-d_6$) δ 12.50 (s, 1H), 7.68–7.59 (m, 2H), 7.26–7.17 (m, 2H), 2.04–1.94 (m, 1H), 1.08–0.96 (m, 2H), 0.80–0.69 (m, 2H); ^{13}C NMR (151 MHz, $\text{DMSO}-d_6$) δ 154.5, 153.9, 148.0, 126.0, 125.2, 120.9, 15.2, 10.2; LCMS m/z 203.1 $[\text{M}+\text{H}]^+$.

5-(4-Isopropylphenyl)-1,3,4-oxadiazol-2(3H)-one (23s)

Prepared by General Methods 1.2, 2 (8 equiv. at 80 °C) and 3 from 4-isopropylbenzoic acid. Isolated as a white solid (190 mg, 33 %).

^1H NMR (600 MHz, $\text{DMSO}-d_6$) δ 12.51 (s, 1H), 7.76–7.66 (m, 2H), 7.41 (d, $J = 8.3$ Hz, 2H), 2.95 (hept, $J = 6.9$ Hz, 1H), 1.22 (d, $J = 6.9$ Hz, 6H); ^{13}C NMR (176 MHz, $\text{DMSO}-d_6$) δ 154.5, 153.9, 152.1, 127.2, 125.3, 121.6, 33.4, 23.5; LCMS m/z 205.0 $[\text{M}+\text{H}]^+$.

5-(4-tert-Butylphenyl)-1,3,4-oxadiazol-2(3H)-one (23t)

Prepared by General Method 3 from 4-tert-butylbenzohydrazide. Isolated as a white solid (123 mg, 91 %).

^1H NMR (600 MHz, $\text{DMSO-}d_6$) δ 12.52 (s, 1H), 7.75–7.68 (m, 2H), 7.59–7.52 (m, 2H), 1.30 (s, 9H); ^{13}C NMR (151 MHz, $\text{DMSO-}d_6$) δ 154.5, 154.3, 153.9, 126.0, 125.1, 121.3, 34.8, 30.8; LCMS m/z 219.1 $[\text{M}+\text{H}]^+$.

5-(4-(Difluoromethyl)phenyl)-1,3,4-oxadiazol-2(3H)-one (23u)

Prepared by General Methods 1.2, 2 (8 equiv. at 70 °C) and 3 from 4-(difluoromethyl)benzoic acid. Isolated as a white solid (165 mg, 54 %).

^1H NMR (600 MHz, $\text{DMSO-}d_6$) δ 12.71 (s, 1H), 7.93 (d, $J = 8.1$ Hz, 2H), 7.74 (d, $J = 8.1$ Hz, 2H), 7.13 (t, $J = 55.6$ Hz, 1H); ^{13}C NMR (176 MHz, $\text{DMSO-}d_6$) δ 154.3, 153.1, 136.5 (t, $J = 22.3$ Hz), 126.6 (t, $J = 6.1$ Hz), 126.2, 125.7, 114.3 (t, $J = 236.5$ Hz); LCMS m/z 211.1 $[\text{M}-\text{H}]^-$.

5-(4-(Trifluoromethyl)phenyl)-1,3,4-oxadiazol-2(3H)-one (23v)

Prepared by General Method 3 from 4-(trifluoromethyl)benzohydrazide. Isolated as a white solid (80 mg, 30 %).

^1H NMR (600 MHz, $\text{DMSO-}d_6$) δ 12.92 – 12.59 (m, 1H), 8.00 (d, $J = 8.6$ Hz, 2H), 7.91 (d, $J = 8.6$ Hz, 2H); ^{13}C NMR (151 MHz, $\text{DMSO-}d_6$) δ 154.4, 152.7, 131.0 (q, $J = 31.8$ Hz), 127.8, 126.3 (q, $J = 3.7$ Hz), 126.1, 123.8 (q, $J = 272.4$ Hz); LCMS m/z 229.1 $[\text{M}-\text{H}]^-$.

5-(4-Cyanophenyl)-1,3,4-oxadiazol-2(3H)-one (23w)

Prepared by General Method 3 from 4-cyanobenzohydrazide. Isolated as a white solid (79 mg, 68 %).

^1H NMR (600 MHz, $\text{DMSO-}d_6$) δ 12.85 (s, 1H), 8.03–7.98 (m, 2H), 7.97–7.92 (m, 2H); ^{13}C NMR (151 MHz, $\text{DMSO-}d_6$) δ 154.3, 152.5, 133.2, 128.0, 125.9, 118.1, 113.4; LCMS m/z 186.0 $[\text{M}-\text{H}]^-$.

5-(4-Methoxyphenyl)-1,3,4-oxadiazol-2(3H)-one (23x)

Prepared by General Method 3 from 4-methoxybenzohydrazide. Isolated as a white solid (138 mg, 60 %).

^1H NMR (600 MHz, $\text{DMSO-}d_6$) δ 12.42 (s, 1H), 7.90–7.52 (m, 2H), 7.32–6.95 (m, 2H), 3.83 (s, 3H); ^{13}C NMR (176 MHz, $\text{DMSO-}d_6$) δ 161.6, 154.5, 153.8, 127.1, 116.3, 114.7, 55.4; LCMS m/z 193.1 $[\text{M}+\text{H}]^+$.

5-(4-Isopropoxyphenyl)-1,3,4-oxadiazol-2(3H)-one (23y)

Prepared by General Method 3 from 4-isopropoxybenzohydrazide. Isolated as a white solid (151 mg, 89 %).

^1H NMR (600 MHz, $\text{DMSO-}d_6$) δ 12.41 (s, 1H), 7.74–7.61 (m, 2H), 7.12–6.97 (m, 2H), 4.71 (hept, $J = 6.0$ Hz, 1H), 1.29 (d, $J = 6.0$ Hz, 6H); ^{13}C NMR (176 MHz, $\text{DMSO-}d_6$) δ 159.9, 154.5, 153.9, 127.1, 116.0, 115.9, 69.6, 21.6; LCMS m/z 221.1 $[\text{M}+\text{H}]^+$.

5-(4-Nitrophenyl)-1,3,4-oxadiazol-2(3H)-one (23aa)

Purchased from Key Organics, GC-0606.

5-(4-(Dimethylamino)phenyl)-1,3,4-oxadiazol-2(3H)-one (23bb)

Prepared by General Methods 2 (8 equiv. at 70 °C) and 3 from ethyl 4-(dimethylamino)benzoate. Isolated as a white solid (45 mg, 8 %).

¹H NMR (600 MHz, DMSO-*d*₆) δ 12.22 (s, 1H), 7.65–7.48 (m, 2H), 6.87–6.65 (m, 2H), 2.99 (s, 6H); ¹³C NMR (176 MHz, CDCl₃) δ 156.4, 154.7, 152.5, 127.3, 111.6, 110.7, 40.2; LCMS *m/z* 206.2 [M+H]⁺.

5-(3,4-Dichlorophenyl)-1,3,4-oxadiazol-2(3H)-one (23cc)

Prepared by General Method 3 from 3,4-dichlorobenzohydrazide. Isolated as a white solid (80 mg, 24 %).

¹H NMR (600 MHz, DMSO-*d*₆) δ 12.79 (s, 1H), 7.97 (d, *J* = 2.0 Hz, 1H), 7.83 (d, *J* = 8.4 Hz, 1H), 7.76 (dd, *J* = 8.4, 2.0 Hz, 1H); ¹³C NMR (151 MHz, DMSO-*d*₆) δ 154.3, 152.0, 134.1, 132.2, 131.7, 127.0, 125.4, 124.6; LCMS *m/z* 229.0 [M-H]⁻.

5-(4-Chloro-3-(trifluoromethyl)phenyl)-1,3,4-oxadiazol-2(3H)-one (23dd)

Prepared by General Methods 1.1, 2 and 3 from 4-chloro-3-(trifluoromethyl)benzoic acid. Isolated as a white solid (229 mg, 40 %).

Mp 158-159 °C; IR ν_{\max} (film) 3078, 2824, 1178, 1748, 1609, 1478, 1297 cm⁻¹; ¹H NMR (700 MHz, DMSO-*d*₆) δ 12.82 (s, 1H), 8.09 – 8.04 (m, 2H), 7.91 (d, *J* = 8.2 Hz, 1H); ¹³C NMR (176 MHz, DMSO-*d*₆) δ 154.2, 152.0, 133.4, 132.9, 130.6, 127.5 (q, *J* = 31.4 Hz), 124.2 (q, *J* = 5.3 Hz), 123.7, 122.3 (q, *J* = 273.3 Hz); LCMS *m/z* 263.0 ([M-H]⁻); HRMS C₉H₄ClF₃N₂O₂: calcd. 263.9908 [M]⁺, found 263.99085.

5-(4-Methyl-3-(trifluoromethyl)phenyl)-1,3,4-oxadiazol-2(3H)-one (23ee)

Prepared by General Methods 2 and 3 from methyl 4-methyl-3-(trifluoromethyl)benzoate. Isolated as a white solid (45 mg, 16 %).

¹H NMR (600 MHz, DMSO-*d*₆) δ 12.69 (s, 1H), 8.00–7.94 (m, 2H), 7.64 (d, *J* = 8.1 Hz, 1H), 2.52 (s, 3H); LCMS *m/z* 243.1 [M-H]⁻.

5-(4-Isopropyl-3-(trifluoromethyl)phenyl)-1,3,4-oxadiazol-2(3H)-one (23ff)

5-[4-Bromo-3-(trifluoromethyl)phenyl]-1,3,4-oxadiazol-2(3H)-one (**32**) was prepared by General Methods 2 and 3 from methyl 4-bromo-3-(trifluoromethyl)benzoate. Isolated as a white solid (429 mg, 79 %).

¹H NMR (400 MHz, DMSO-*d*₆) δ 12.83 (s, 1H), 8.08 (d, *J* = 8.4 Hz, 1H), 8.05 (d, *J* = 2.0 Hz, 1H), 7.95 (dd, *J* = 8.4, 2.0 Hz, 1H); LCMS *m/z* 306.9 [M-H]⁻.

A thick-walled reaction vial was charged with Pd(dppf)Cl₂·DCM (26 mg, 0.03 mmol, 0.05 equiv.), 2-isopropenyl-4,4,5,5-tetramethyl-1,3,2-dioxaborolane (0.12 mL, 0.64 mmol, 1.2 equiv.) and **32** (164 mg, 0.53 mmol). 1,4-Dioxane (5 mL) and an aqueous solution of K₂CO₃ (0.56 mL, 2 N, 1.11 mmol) were added, the vial was purged with Ar and then heated at 100 °C for 16 h. The solvents were evaporated and the residue dissolved in a

minimum volume of DMSO. Purification by chromatography (0-100% MeCN in H₂O, 0.1% NH₄OH modifier) to give 5-[4-isopropenyl-3-(trifluoromethyl)phenyl]-1,3,4-oxadiazol-2(3*H*)-one (**33**) (84 mg, 59 %) as a white solid.

¹H NMR (700 MHz, DMSO-*d*₆) δ 7.99 – 7.92 (m, 2H), 7.54 – 7.50 (m, 1H), 5.33 – 5.28 (m, 1H), 4.88 (brs, 1H), 2.05 (s, 3H); LCMS *m/z* 269.2 [M-H]⁻.

Hydrogenation of **33** to **23ff** was performed in a COware gas reactor. To chamber 1 was added **33** (80 mg, 0.30 mmol), 10 % Pd/C (32 mg, 0.03 mmol) and EtOH (4 mL). To chamber 2 was added flakes of zinc (270 mg, 4.14 mmol). The H-Cap was secured tightly on the top of chamber 1 and the system was purged with N₂. Aqueous HCl (1.18 mL, 4 M, 4.74 mmol) was added to chamber 2, the system was securely sealed, and the two chambers were stirred for 18 h. The residual pressure was carefully released and the reaction mixture from chamber 1 was filtered and concentrated under reduced pressure. The residue was purified by chromatography (0-100 % MeCN in H₂O, 0.1% NH₄OH modifier) to give **23ff** (64 mg, 79 %) as a white solid.

¹H NMR (700 MHz, DMSO-*d*₆) δ 12.65 (s, 1H), 8.01 (dd, *J* = 8.3, 1.7 Hz, 1H), 7.92 (d, *J* = 1.8 Hz, 1H), 7.83 (d, *J* = 8.3 Hz, 1H), 3.25 (dt, *J* = 13.3, 6.7 Hz, 1H), 1.25 (d, *J* = 6.7 Hz, 6H); ¹³C NMR (176 MHz, DMSO-*d*₆) δ 154.6, 152.7, 150.6, 129.3, 129.1, 126.8 (q, *J* = 29.6 Hz), 124.0 (q, *J* = 274.1 Hz), 122.3, 121.9 (q, *J* = 6.1 Hz), 29.2, 23.6; LCMS *m/z* 271.2 [M-H]⁻.

5-(4-Cyclopropyl-3-(trifluoromethyl)phenyl)-1,3,4-oxadiazol-2(3*H*)-one (23gg)

Prepared by General Methods 1.2, 2 (15 equiv. at 100 °C) and 3 from 4-cyclopropyl-3-(trifluoromethyl)benzoic acid.²⁴ Isolated as a white solid (68 mg, 61 %).

¹H NMR (600 MHz, DMSO-*d*₆) δ 12.68 (s, 1H), 7.92 (m, 2H), 7.31 (d, *J* = 8.2 Hz, 1H), 2.16 (m, 1H), 1.17–1.10 (m, 2H), 0.93–0.86 (m, 2H); ¹³C NMR (176 MHz, DMSO-*d*₆) δ 154.3, 152.7, 145.7, 129.2, 128.5 (q, *J* = 30.1 Hz), 126.7, 124.1 (q, *J* = 274.1 Hz), 122.0 (q, *J* = 6.0 Hz), 121.5, 12.1 (d, *J* = 2.3 Hz), 10.1; LCMS *m/z* 269.1 [M-H]⁻.

5-(3-Cyclopropyl-4-(trifluoromethyl)phenyl)-1,3,4-oxadiazol-2(3*H*)-one (23hh)

Prepared by General Methods 1.2, 2 (8 equiv. at 70 °C) and 3 from 3-cyclopropyl-4-(trifluoromethyl)benzoic acid.²⁴ Isolated as a white solid (88 mg, 51 %).

¹H NMR (600 MHz, DMSO-*d*₆) δ 12.78 (s, 1H), 7.84 (d, *J* = 8.3 Hz, 1H), 7.75 (d, *J* = 8.3 Hz, 1H), 7.43 (s, 1H), 2.22–2.11 (m, 1H), 1.16–1.04 (m, 2H), 0.92–0.79 (m, 2H); ¹³C NMR (176 MHz, DMSO-*d*₆) δ 154.3, 152.7, 143.1, 130.0 (q, *J* = 29.4 Hz), 127.9, 126.8 (q, *J* = 5.7 Hz), 124.2 (q, *J* = 273.9 Hz), 122.7, 122.3, 12.0 (d, *J* = 2.4 Hz), 9.2; LCMS *m/z* 269.2 [M-H]⁻.

5-(4-(Dimethylamino)-3-(trifluoromethyl)phenyl)-1,3,4-oxadiazol-2(3*H*)-one (23ii)

Prepared by General Methods 2 (4 equiv. at 80 °C) and 3 from methyl 4-(dimethylamino)-3-(trifluoromethyl)benzoate.²⁴ Isolated as a white solid (212 mg, 44 %).

¹H NMR (700 MHz, DMSO-*d*₆) δ 7.91 (dd, *J* = 8.6, 2.0 Hz, 1H), 7.88 (d, *J* = 2.0 Hz, 1H), 7.46 (d, *J* = 8.7 Hz, 1H), 2.80 (s, 6H); ¹³C NMR (176 MHz, DMSO-*d*₆) δ 155.1, 154.3, 152.8, 129.7, 124.6 (q, *J* = 5.7 Hz), 123.9 (q, *J* = 273.1 Hz), 122.3, 121.2 (q, *J* = 29.6 Hz), 117.3, 44.4, 44.4; LCMS *m/z* 274.2 [M+H]⁺.

5-(1-Methylindolin-5-yl)-1,3,4-oxadiazol-2(3H)-one (23jj)

Prepared by General Methods 2 (8 equiv. at 45 °C) and 3 from methyl 1-methylindoline-5-carboxylate.²⁴ Isolated as an off-white solid (60 mg, 87 %).

¹H NMR (600 MHz, DMSO-*d*₆) δ 12.19 (s, 1H), 7.44 (dd, *J* = 8.2, 1.7 Hz, 1H), 7.40 (d, *J* = 1.3 Hz, 1H), 6.53 (d, *J* = 8.3 Hz, 1H), 3.41 (t, *J* = 8.4 Hz, 2H), 2.95 (t, *J* = 8.4 Hz, 2H), 2.78 (s, 3H); ¹³C NMR (176 MHz, DMSO-*d*₆) δ 155.5, 154.8, 154.6, 130.6, 125.9, 120.9, 111.8, 105.7, 54.7, 34.4, 27.4; LCMS *m/z* 218.1 [M+H]⁺.

5-(1-Methylindolin-6-yl)-1,3,4-oxadiazol-2(3H)-one (23kk)

Prepared by General Methods 2 (15 equiv. at 100 °C) and 3.2 from methyl 1-methylindoline-6-carboxylate.²⁴ Isolated as a white solid (63 mg, 56 %).

¹H NMR (400 MHz, DMSO-*d*₆) δ 12.46 (s, 1H), 7.16 (d, *J* = 7.6 Hz, 1H), 7.02 (dd, *J* = 7.5, 1.5 Hz, 1H), 6.79 (d, *J* = 1.3 Hz, 1H), 3.35–3.30 (m, 2H), 2.93 (t, *J* = 8.3 Hz, 2H), 2.75 (s, 3H); ¹³C NMR (176 MHz, DMSO-*d*₆) δ 154.5, 154.5, 153.7, 134.2, 124.5, 123.0, 114.9, 102.3, 55.2, 35.2, 28.0; LCMS *m/z* 218.1 [M+H]⁺.

5-(1,4-Dimethyl-1,2,3,4-tetrahydroquinolin-6-yl)-1,3,4-oxadiazol-2(3H)-one (23ll)

Prepared by General Methods 2 (15 equiv. at 120 °C) and 3 from methyl 1,4-dimethyl-2,3-dihydroquinoline-6-carboxylate.²⁴ Isolated as a white solid (79 mg, 72 %).

¹H NMR (600 MHz, DMSO-*d*₆) δ 12.18 (s, 1H), 7.02 (dd, *J* = 8.3, 2.0 Hz, 1H), 6.72 (d, *J* = 1.9 Hz, 1H), 6.50 (d, *J* = 8.4 Hz, 1H), 3.40 (dd, *J* = 5.7, 4.1 Hz, 2H), 3.26 (dd, *J* = 5.7, 4.1 Hz, 2H), 2.88 (s, 3H), 2.82 (s, 3H); ¹³C NMR (176 MHz, DMSO-*d*₆) δ 155.0, 154.7, 139.3, 136.2, 116.4, 111.8, 109.0, 105.7, 48.9, 48.3, 38.7, 38.4; LCMS *m/z* 247.2 [M+H]⁺.

5-(4-Chlorophenyl)isoxazol-3(2H)-one (24)

NH₂OH.HCl (0.15 mL, 3.6 mmol, 3.0 equiv.) was added to a solution of ethyl 3-(4-chlorophenyl)propionate (250 mg, 1.2 mmol) and NaOH (48 mg, 1.2 mmol, 1.0 equiv.) in EtOH (4mL) and H₂O (4mL) at RT. The reaction mixture was stirred for 16 h, then acidified to pH 2 with aqueous HCl (2 N). The EtOH was removed under reduced pressure and the aqueous residue extracted with EtOAc (3 x 20 mL). The combined organic extracts were dried (Na₂SO₄) and evaporated under reduced pressure. The residue was purified by silica gel chromatography (0-10 % MeOH in CH₂Cl₂) to give **24** (12 mg, 5 %) as an off-white solid.

¹H NMR (600 MHz, DMSO-*d*₆) δ 11.46 (s, 1H), 7.92 – 7.74 (m, 2H), 7.65 – 7.47 (m, 2H), 6.62 (s, 1H); LCMS *m/z* 196.1 [M+H]⁺.

5-(4-Chlorophenyl)-1,3,4-thiadiazol-2(3H)-one (25)

Prepared by General Method 4 from 4-chlorobenzohydrazide. Isolated as a white solid (25 mg, 13 %).

^1H NMR (700 MHz, $\text{DMSO-}d_6$) δ 13.19 (s, 1H), 7.75 – 7.66 (m, 2H), 7.60 – 7.54 (m, 2H); ^{13}C NMR (176 MHz, $\text{DMSO-}d_6$) δ 171.1, 150.3, 135.3, 129.4, 129.3, 127.4; LCMS m/z 211.1 $[\text{M-H}]^-$.

5-(4-Chloro-3-(trifluoromethyl)phenyl)-1,3,4-thiadiazol-2(3H)-one (26)

Prepared by General Method 4 from 4-chloro-3-(trifluoromethyl)benzohydrazide. Isolated as a white solid (10 mg, 8 %) as a white solid.

^1H NMR (600 MHz, CDCl_3) δ 9.50 (s, 1H), 8.01 (d, $J = 2.1$ Hz, 1H), 7.76 (dd, $J = 8.4, 2.1$ Hz, 1H), 7.61 (d, $J = 8.4$ Hz, 1H); LCMS m/z 279.0 $[\text{M-H}]^-$.

5-(4-Chloro-3-(trifluoromethyl)phenyl)-1,3,4-oxadiazole (27)

p -TsOH.H₂O (28 mg, 0.15 mmol 0.3 equiv.) was added to a thick-walled reaction vial (20 mL) containing HC(OEt)_3 (1.0 mL, 6.5 mmol, 15 equiv.) and 4-chloro-3-(trifluoromethyl)benzohydrazide (100 mg, 0.42 mmol) under N_2 . The vial was sealed, slowly warmed to 50 °C and then stirred for 30 min (vigorous bubbling was observed). The mixture was cooled to RT, and added dropwise to a beaker containing a stirred solution of saturated aqueous NaHCO_3 (20 mL). The aqueous mixture was extracted with CH_2Cl_2 (50 ml), and the organic phase was separated, dried and concentrated under reduced pressure. The residue was purified by chromatography on silica gel (30 % EtOAc in cyclohexane) to give **27** (66 mg, 63 %).

^1H NMR (600 MHz, $\text{DMSO-}d_6$) δ 9.45 (s, 1H), 8.34 (d, $J = 2.0$ Hz, 1H), 8.31 (dd, $J = 8.3, 2.0$ Hz, 1H), 8.00 (d, $J = 8.3$ Hz, 1H); LCMS m/z 249.1 $[\text{M+H}]^+$.

Notum protein expression and purification

Methods have been described in detail in reference 18. In brief, human Notum (UniProtKB ID: Q6P988) enzyme core sequence comprising amino acids S81–T451 with a C330S mutation was cloned into a stable cell line vector pNeo_sec. A stable HEK293S GNTI- cell line was obtained and used for protein production as described previously. The cells were expanded and grown in roller bottles (Greiner). The conditioned media were dialyzed and passed through a 5 ml HisTrap Excel column (GE Healthcare), followed by 20 mM imidazole PBS wash. Notum protein was eluted with 300 mM imidazole PBS. To remove flexible glycans, the protein was deglycosylated with endo- β -N-acetylglucosaminidase F1 (37°C, 1 hour) and further purified by size-exclusion chromatography (Superdex 200 16/60 column, GE Healthcare) in 10 mM Hepes, pH 7.4, 150 mM NaCl buffer.

Notum OPTS biochemical assay

Methods have been described in detail in reference 18. A Labcyte Echo 550 acoustic liquid handler was used to dispense 500 nL of test compound into 384-well plates (Greiner catalog #781076). 25 μ L of 2 μ M trisodium 8-octanoyloxyppyrene-1,3,6-trisulfonate (OPTS, Sigma #74875) solution in 50 mM Tris, 5 mM CaCl₂, 0.5 mM MgCl₂, pH 7.4 assay buffer was added to each well, followed by 25 μ L of 2.38 nM Notum carboxyesterase enzyme solution. Plates were incubated for 40 minutes at room temperature, and endpoint fluorescence was measured on a PheraSTAR FSX microplate reader with an excitation wavelength of 485 nm and emission wavelength of 520 nm. Plates were quality controlled based on a signal window greater than three-fold between DMSO and positive control compound, and a Z prime greater than 0.5.

Dose-response curve analysis: Plate layout and measured fluorescence values were input into Dotmatics Studies data management tool. After implementing Quality Control with a cut-off of Z prime values higher than 0.5, compound IC₅₀ values were calculated from curves using a 4PL fit and compared between technical replicates. Final potency values implied an $n \geq 2$ with IC₅₀ within 0.5-2x between replicates. For representative curves, see **Figure S6**.

Data analysis: IC₅₀ values presented in Tables 1-4 are mean \pm SD ($n = 2-8$).

TCF/LEF reporter (Luciferase) cell based assay

Described in detail in reference 16. An aliquot of 20 μ L of TCF LEF cells were plated in 384 well cell culture Greiner microplates (catalog #781098) at 10,000 cells per well and incubated overnight at 37 °C. An Echo liquid handler was used to acoustically dispense 150 nL of compounds into V-well polypropylene Greiner microplate (catalog #781280) to create a 10-point curve. 25 μ L of 0.5 % DMEM media (500 mL DMEM 1X GlutaMax, 4.5

g/L D-Glucos, Pyruvate plus 2.5 mL 10 % Fetal Bovine Serum and 5 mL Penicillin Streptomycin) was added to the Wnt compound plates and 25 μ L of Notum at 1000 μ g/mL was added to the Notum compound plates and incubated at room temperature for 10 minutes. 25 μ L of Wnt-3A at 200 ng/mL was added to all plates and incubated at room temperature for 1 hour. 20 μ L of media was aspirated from the cell plates using a CyBio SELMA followed the addition of 40 μ L from the compound plates. After an overnight incubation at 37 °C, GFP fluorescence was measured on a PHERAstar FSX microplate reader with a wavelength of 458 nm and emission wavelength of 520 nm. 20 μ L of steady-glo luciferase assay buffer (Promega #E2520) was added to the cell plates using a CyBio, the luminescence was measured on the PHERAstar.

Molecular docking

Compound design was aided by molecular docking. Docking was conducted using Schrödinger Glide. Schrödinger Release 2018-3: Glide, Schrödinger, LLC, New York, NY, 2018.

In vitro ADME screens

Selected compounds were screened for aqueous solubility, transit performance in MDCK-MDR1 cell lines for permeability, and metabolic stability in liver microsomes as a measure of clearance. Assay protocols and additional data is presented in the Supporting Information **Figure S3**. ADME studies reported in this work were independently performed by GVK Biosciences (Hyderabad, India) or Cyprotex (Macclesfield, UK).

pK_a determination

The pK_as were determined using the spectrometric (UV-metric) technique and were performed by Cyprotex (Macclesfield, UK).

Compound **23aa**: The sample was titrated in a UV-metric triple titration from pH 2.0 – 12.0 at concentrations of 31 – 19 μ M, under methanol-water co-solvent conditions (the methanol mixing ratio varied from 48.9 to 29.6 % w/w). No precipitation of the sample from solution was observed. One pK_a, with an aqueous value of 6.44 \pm 0.08, was determined from the spectroscopic data collected by Yasuda-Shedlovsky extrapolation of the individual results obtained.

Compound **23bb**: The sample was titrated in three UV-metric single titrations from pH 1.5 – 12.5 at concentrations of 29 – 23 μ M, under methanol-water co-solvent conditions (the methanol mixing ratio varied from 47.9 to 30.7 % w/w). No precipitation of the sample from solution was observed. Two pK_as, with aqueous values of 2.92 \pm 0.06 and 7.42 \pm 0.01, were determined from the spectroscopic data collected by Yasuda-Shedlovsky extrapolation of the individual results obtained.

Compound **23dd**: The sample was titrated in a UV-metric triple titration from pH 2.0 – 12.0 at concentrations of 32 – 23 μM , under aqueous conditions. No precipitation of the sample from solution was observed. One pK_a , with an average value of 6.72 ± 0.01 , was determined from the spectroscopic data collected.

Mouse pharmacokinetic studies

In vivo mouse pharmacokinetic data was generated at GVK Biosciences (Hyderabad, India). Assay protocols and additional data is presented in the Supporting Information **Figure S4**.

ASSOCIATED CONTENT

Supporting Information

The Supporting Information is available free of charge on the ACS Publications website at ...

X-ray structure determination: methods, data collection and refinement statistics. Plot of Notum pIC₅₀ vs clog*P* and Lipophilic Fragment Constant (π). Notum occupancy assay with FP-Biotin. ADME protocols and additional data. Mouse Pharmacokinetic data for **23dd**. Analytical and spectral data for **23dd**. Notum OPTS and TCF/LEF screening data for **23dd**. Comparison of profile of **23dd** with **2**.

Molecular formula strings (CSV)

Accession Codes

Coordinates for X-ray structures of Notum crystallized with **7** (6ZUV) and **23dd** (6ZVL) have been deposited in the Protein data Bank.

AUTHOR INFORMATION

Corresponding Authors

EYJ: Phone: +44 (0)1865 287546; E-mail: yvonne@strubi.ox.ac.uk. Orchid: 0000-0002-3834-1893.

PVF: Phone: +44 (0)20 7679 6971; E-mail: p.fish@ucl.ac.uk. Orchid: [0000-0002-2117-2173](https://orcid.org/0000-0002-2117-2173).

Authors

William Mahy: E-mail: willmahy123@gmail.com

Nicky J. Willis: E-mail: n.willis@ucl.ac.uk

Yuguang Zhao: E-mail: yuguang@strubi.ox.ac.uk. Orchid: 0000-0001-8916-8552.

Hannah L. Woodward: E-mail: hannah.woodward@ucl.ac.uk. Orchid: 0000-0001-8429-2546.

Fredrik Svensson: E-mail: f.svensson@ucl.ac.uk. Orchid: 0000-0002-5556-8133.

James Siphthorp: E-mail: j.siphthorp@imperial.ac.uk

Luca Vecchia: E-mail: luca.vecchia@kellogg.ox.ac.uk

Reinis R. Ruza: E-mail: reinis.ruza@balliol.ox.ac.uk

James Hillier: E-mail: jameshillier93@gmail.com

Svend Kjaer: E-mail: Svend.Kjaer@crick.ac.uk

Sarah Frew: E-mail: s.frew@ucl.ac.uk

Amy Monaghan: E-mail: amy.monaghan@ucl.ac.uk

Magda Bictash: E-mail: m.bictash@ucl.ac.uk

Patricia Salinas: E-mail: p.salinas@ucl.ac.uk

Paul Whiting: E-mail: p.whiting@ucl.ac.uk

Jean-Paul Vincent: E-mail: JP.Vincent@crick.ac.uk

Notes

† These authors contributed equally.

The authors declare no competing financial interest.

ACKNOWLEDGEMENTS

We thank our colleagues Stefano Benvegna, Jamie Bilsland, Sarah Jolly, Ernest Palomer, Morgan Roberts and Laura Schuhmacher of our Notum Consortium for their support and advice. The Cell Services and Structural Biology Science Technology Platforms (STPs) at the Francis Crick Institute are gratefully acknowledged for their provision and purification of recombinant Notum. We thank staff at Diamond Light Source for assistance with x-ray data collection and the UCL Department of Chemistry for spectroscopic and analytical services. ADME studies reported in this work were independently performed by GVK Biosciences (Hyderabad, India) or Cyprotex (Macclesfield, UK). Mouse PK studies were performed by GVK Biosciences (Hyderabad, India).

This work was supported by Alzheimer's Research UK (ARUK), the Francis Crick Institute and Eli Lilly. The ARUK UCL Drug Discovery Institute is core funded by Alzheimer's Research UK (520909). The Francis Crick Institute receives its core funding from Cancer Research UK (FC001002), the UK Medical Research Council (FC001002), and the Wellcome Trust (FC001002). Structural analysis was performed by Y.Z., L.V., R.R.R. and E.Y.J. supported by Cancer Research UK (Programme Grant C375/A17721). The Wellcome Trust funds the Wellcome Centre for Human Genetics, University of Oxford (Centre Grant 203141/Z/16/Z).

ABBREVIATIONS

ABC transporters, ATP-binding cassette transporters; ABPP, activity-based protein profiling; AD, Alzheimer's disease; ADME, absorption distribution metabolism elimination; BBB, blood-brain barrier; BCRP, breast cancer resistance protein; CNS, central nervous system; DMF, *N,N*-dimethylformamide; DMSO, dimethylsulfoxide; ER, efflux ratio; HLM, human liver microsomes; HTS, high throughput screen; LE, ligand efficiency; LLE, lipophilic ligand efficiency; MLM, mouse liver microsomes; MPO, multiparameter optimization; MRP, multidrug resistance-associated protein; OPTS, trisodium 8-octanoyloxypyrene-1,3,6-trisulfonate; PDB, Protein Data Bank; P-gp, P-glycoprotein; PD, pharmacodynamics; PK, pharmacokinetic; RT, room temperature; SAR, structure activity relationship; SBDD, structure-based drug design; THF, tetrahydrofuran; TPSA, topological polar surface area.

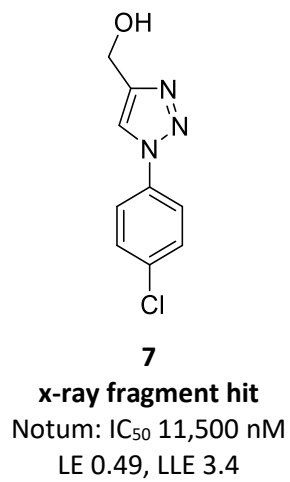
REFERENCES and NOTES

1. Clevers, H., Nusse, R. Wnt/ β -catenin signaling and disease. *Cell*, **2012**, *149*, 1192-1205.
2. Krishnamurthy, N., Kurzrock, R. Targeting the Wnt/beta-catenin pathway in cancer: Update on effectors and inhibitors. *Cancer Treat. Rev.* **2018**, *62*, 50-60.
3. Baron R., Gori, F. Targeting WNT signaling in the treatment of osteoporosis. *Curr. Opin. Pharmacol.* **2018**, *40*, 134-141.
4. Zhong, Z. Virshup, D.M. Wnt signalling and drug resistance in cancer. *Mol. Pharmacol.* **2020**, *97*, 72-89.
5. Kakugawa, S., Langton, P.F., Zebisch, M., Howell, S., Chang, T.H., Liu, Y., Feizi, T., Bineva, G., O'Reilly, N., Snijders, A.P., Jones, E.Y., Vincent, J.P. NOTUM deacylates Wnt proteins to suppress signaling activity. *Nature* **2015**, *519*, 187-192.
6. Movérare-Skrtic, S., Nilsson, K.H., Henning, P., Funck-Brentano, T., Nethander, M., Rivadeneira, F., Coletto Nunes, G., Koskela, A., Tuukkanen, J., Tuckermann, J., Perret, C., Souza, P.P.C., Lerner, U.H., Ohlsson, C. Osteoblast-derived NOTUM reduces cortical bone mass in mice and the *NOTUM* locus is associated with bone mineral density in humans. *FASEB J.* **2019**, *33*, 11163-11179.
7. Brommage, R., Liu, J., Vogel, P., Mseeh, F., Thompson, A.Y., Potter, D.G., Shadoan, M.K., Hansen, G.M., Jeter-Jones, S., Cui, J., Bright, D., Bardenhagen, J.P., Doree, D.D., Moverare-Skrtic, S., Nilsson, K.H., Henning, P., Lerner, U.H., Ohlsson, C., Sands, A.T., Tarver, J.E., Powell, D.R., Zambrowicz, B., Liu, Q. NOTUM inhibition increases endocortical bone formation and bone strength. *Bone Research* **2019**, *7*, 2.
8. Pentimikko, N., Iqbal, S., Mana, M., Andersson, S., Cognetta III, A.B., Suci, R.M., Roper, J., Luopajarvi, K., Markelin, E., Gopalakrishnan, S., Smolander, O.-P., Naranjo, S., Saarinen, T., Juuti, A., Pietiläinen, K., Auvinen, P., Ristimäki, A., Gupta, N., Tammela, T., Jacks, T., Sabatini, D.M., Cravatt, B.F., Yilmaz, O.H., Katajisto, P. Notum produced by Paneth cells attenuates regeneration of aged intestinal epithelium. *Nature* **2019**, *571*, 398-402.
9. McLeod, F., Salinas, P.C. Wnt proteins as modulators of synaptic plasticity. *Curr. Opin. Neurobiol.* **2018**, *53*, 90-95.
10. Palomer, E., Buechler, J., Salinas, P.C. (2019). Wnt signaling deregulation in the aging and Alzheimer's brain. *Front. Cell. Neurosci.* **2019**, *13*, 227.
11. Mizrak, D., Bayin, N.S., Yuan, J., Liu, Z., Suci, R.M., Niphakis, M.J., Ngo, N., Lum, K.M., Cravatt, B.F., Joyner, A.L., Sims, P.A. Single-cell profiling and SCOPE-Seq reveal lineage dynamics of adult ventricular-subventricular zone neurogenesis and NOTUM as a key regulator. *Cell Rep.* **2020**, *31*, 107805.
12. Beckervordersandforth, R., Rolando, C. Untangling human neurogenesis to understand and counteract brain disorders. *Curr. Opin. Pharmacol.* **2019**, *50*, 67-73.
13. Tarver Jr, J.E., Pabba, P.K., Barbosa, J., Han, Q., Gardyan, M.W., Brommage, R., Thompson, A.Y., Schmidt, J.M., Wilson, A.G.E., He, W., Lombardo, V.K., Carson, K.G. Stimulation of cortical bone formation with

- thienopyrimidine based inhibitors of NOTUM pectinacetyltransferase. *Bioorg. Med. Chem. Lett.* **2016**, *26*, 1525–1528.
14. Atkinson, B.N., Steadman, D., Mahy, W., Zhao, Y., Siphthorp, J., Bayle, E. D., Svensson, F., Papageorgiou, G., Jeganathan, F., Frew, S., Monaghan, A., Bictash, M., Jones, E.Y., Fish, P.V. Scaffold-hopping identifies furano[2,3-*d*]pyrimidine amides as potent Notum inhibitors. *Bioorg. Med. Chem. Lett.* **2020**, *30*, 126751.
 15. Suciu, R.M., Cognetta, A.B., Potter, Z.E., Cravatt, B.F. Selective irreversible inhibitors of the Wnt-deacylating enzyme NOTUM developed by activity-based protein profiling. *ACS Med. Chem. Lett.* **2018**, *9*, 563–568.
 16. Atkinson, B.N., Steadman, D., Zhao, Y., Siphthorp, J., Vecchia, L., Ruza, R.R., Jeganathan, F., Lines, G., Frew, S., Monaghan, A., Kjaer, S., Bictash, M., Jones, E.Y., Fish, P.V. Discovery of 2-phenoxyacetamides as inhibitors of the Wnt-depalmitoleating enzyme NOTUM from an X-ray fragment screen. *Med. Chem. Commun.* **2019**, *10*, 1361-1369.
 17. Zhao, Y., Ren, J., Hillier, J., Jones, M., Lu, W., Jones, E.Y. Structural characterisation of melatonin as an inhibitor of the Wnt deacylase Notum. *J. Pineal Res.* **2020**, *68*, e12630.
 18. Mahy, W., Patel, M., Steadman, D., Woodward, H.L., Atkinson, B.N., Svensson, F., Willis, N.J., Flint, A., Papatheodorou, D., Zhao, Y., Vecchia, L., Ruza, R.R., Hillier, J., Frew, S., Monaghan, A., Costa, A., Bictash, M., Walter, M.W., Jones, E.Y., Fish, P.V. Screening of a custom-designed acid fragment library identifies 1-phenylpyrroles and 1-phenylpyrrolidines as inhibitors of Notum carboxylesterase activity. *J. Med. Chem.* **2020**, *63*, 9464-9483.
 19. Zhao, Y., Ren, J., Hillier, J., Lu, W., Jones, E.Y. Caffeine inhibits Notum activity by binding at the catalytic pocket. *Commun. Biol.* **2020**, *3*, 555.
 20. Willis, N.J., Bayle, E.D., Papageorgiou, G., Steadman, D., Atkinson, B.N., Mahy, W., Fish, P.V. An improved, scalable synthesis of Notum inhibitor LP-922056 using 1-chloro-1,2-benziodoxol-3-one as a superior electrophilic chlorinating agent. *Beilstein J. Org. Chem.* **2019**, *15*, 2790-2797.
 21. <https://www.diamond.ac.uk/Instruments/Mx/Fragment-Screening/Fragment-Libraries/DSI-poised-library.html>. Accessed May 1, 2020.
 22. Hopkins, A.L., Keseru, G.M., Leeson, P.D., Rees, D.C., Reynolds, C.H. The role of ligand efficiency metrics in drug discovery. *Nat. Rev. Drug Disc.* **2014**, *13*, 105-121.
 23. Johnson, T. W., Gallego, R. A., Edwards, M. P. Lipophilic efficiency as an important metric in drug design. *J. Med. Chem.* **2018**, *61*, 6401-6420.
 24. Fish P.V., Mahy, W., Willis, N.J., Woodward, H., Atkinson, B.N., Bayle, E.D., Siphthorp, J., Jones, E.Y., Zhao, Y., Vecchia, L., Ruza, R.R. Inhibitors of Secreted Carboxy Esterase Notum and their use in Increasing Wnt Protein Signalling and Treatment of Central Nervous System and Other Disorders. WO Patent Application 2020043866, Mar 5, 2020.

25. For recent reviews, see: (a) Verma, G., Khan, M.F., Akhtar, W., Alam, M.M., Akhtar, M., Shaquiquzzaman, M. A review exploring therapeutic worth of 1,3,4-oxadiazole tailored compounds. *Mini Rev. Med. Chem.* **2019**, *19*, 477-509; (b) Sun, J., Makawana, J.A., Zhu, H.L. 1,3,4-Oxadiazole derivatives as potential biological agents. *Mini Rev. Med. Chem.* **2013**, *13*, 1725-1743.
26. Acidic pK_a values for CNS drugs rarely fall below 6.0, see: (a) Manallack, D. T. The pK_a distribution of drugs: application to drug discovery. *Persp. Med. Chem.* **2007**, *1*, 25-38; (b) Manallack, D. T. The acid-base profile of a contemporary set of drugs: implications for drug discovery. *SAR QSAR Environ. Res.* **2009**, *20*, 611-655.
27. There is a paucity of acids with pK_a values between 6 and 7, probably due to the dominance of carboxylic acids and phenols, and the pK_a values usually encountered for these groups, see: Manallack, D. T., Pranker, R. J., Yuriev, E., Opera, T. I., Chalmers, D. K. The significance of acid/base properties in drug discovery. *Chem Soc. Rev.* **2013**, *42*, 485-496.
28. 5-Phenyl-1,3,4-oxadiazole-2(3H)-one [1199-02-6]: predicted pK_a 5.8 ± 0.7 (most acidic) calculated using ACD/Labs software v11.02; predicted pK_a 7.1 (most acidic) calculated using Schrödinger Release 2019-3: Jaguar pK_a , Schrödinger, LLC, New York, NY, 2019. The Jaguar program calculated preference for the 1,3,4-oxadiazol-2(3H)-one tautomer by 20.2 kcal/mol (gas phase by DFT LACVP** B3LPY-D3).
29. Rankovic, Z. CNS drug design: balancing physicochemical properties for optimal brain exposure. *J. Med. Chem.* **2015**, *58*, 2584-2608.
30. Wager, T.T., Hou, X., Verhoest, P.R., Villalobos, A. Moving beyond rules: the development of a central nervous system multiparameter optimization (CNS MPO) approach to enable alignment of druglike properties. *ACS Chem. Neurosci.* **2010**, *1*, 435-449.
31. Liu, Y., Patricelli, M. P., Cravatt, B. F. Activity-based protein profiling: The serine hydrolases. *Proc. Natl. Acad. Sci. USA* **1999**, *96*, 14694-14699.
32. Qosa, H., Miller, D.S., Pasinelli, P., Trotti, D. Regulation of ABC efflux transporters at blood-brain barrier in health and neurological disorders. *Brain Res.* **2015**, *1628*, 298-316.

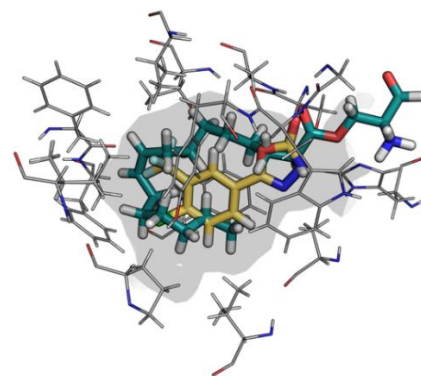
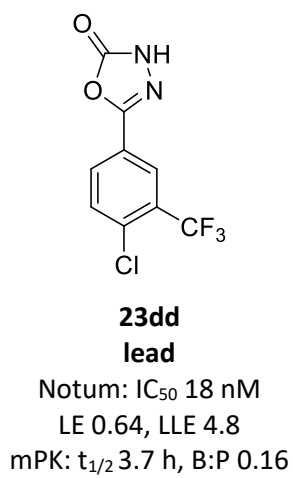
Table of Contents Graphic



**SBDD
SAR evolution**



**properties for
BBB**



Overlay of **23dd** and *O*-palmitoleoyl serine Notum x-ray structures